INFORMATION TO USERS

This manuscript has been reproduced from the microfilm master. UMI films the text directly from the original or copy submitted. Thus, some thesis and dissertation copies are in typewriter face, while others may be from any type of computer printer.

The quality of this reproduction is dependent upon the quality of the copy submitted. Broken or indistinct print, colored or poor quality illustrations and photographs, print bleedthrough, substandard margins, and improper alignment can adversely affect reproduction.

In the unlikely event that the author did not send UMI a complete manuscript and there are missing pages, these will be noted. Also, if unauthorized copyright material had to be removed, a note will indicate the deletion.

Oversize materials (e.g., maps, drawings, charts) are reproduced by sectioning the original, beginning at the upper left-hand corner and continuing from left to right in equal sections with small overlaps.

Photographs included in the original manuscript have been reproduced xerographically in this copy. Higher quality 6" x 9" black and white photographic prints are available for any photographs or illustrations appearing in this copy for an additional charge. Contact UMI directly to order.

ProQuest Information and Learning
300 North Zeeb Road, Ann Arbor, MI 48106-1346 USA
800-521-0600

Université d'Ottawa · University of Ottawa

Adaptive Multiple Sub-band Common Mode RFI Suppression

Pierre D. Lefebvre

A Thesis Submitted to the School of Graduate Studies and Research
in Partial Fulfillment of the Requirements for the Degree of

Master of Applied Science
in Electrical Engineering

Ottawa-Carleton Institute for Electrical and Computer Engineering

School of Information Technology and Engineering
(Electrical and Computer Engineering)

April, 2000

© 2000, Pierre Lefebvre, Ottawa, Canada

National Library of Canada
Acquisitions and Bibliographic Services
395 Wellington Street
Ottawa ON K1A 0N4
Canada

Bibliothèque nationale du Canada
Acquisitions et services bibliographiques
395, rue Wellington
Ottawa ON K1A 0N4
Canada

Your file Votre référence

Our file Notre référence

The author has granted a non-exclusive licence allowing the National Library of Canada to reproduce, loan, distribute or sell copies of this thesis in microform, paper or electronic formats.

L'auteur a accordé une licence non exclusive permettant à la Bibliothèque nationale du Canada de reproduire, prêter, distribuer ou vendre des copies de cette thèse sous la forme de microfiche/film, de reproduction sur papier ou sur format électronique.

The author retains ownership of the copyright in this thesis. Neither the thesis nor substantial extracts from it may be printed or otherwise reproduced without the author's permission.

L'auteur conserve la propriété du droit d'auteur qui protège cette thèse. Ni la thèse ni des extraits substantiels de celle-ci ne doivent être imprimés ou autrement reproduits sans son autorisation.

0-612-58475-5

Canada

Abstract

Currently, the presence of significant RFI noise on twisted pair loops prevents mass deployment of high-speed Digital Subscriber Loop (DSL) technology. DSL technology generally uses bandwidth within the frequency spectrum range of 10 kHz up to 10 MHz. Unfortunately this same spectrum is presently allocated for private, governmental and public radio communications. As well, due to limited cable balance, twisted pair copper cables are highly susceptible to ingress from noise sources present within the DSL frequency bandwidth.

This thesis presents a new architecture to reduce radio frequency interference (RFI) noise at the receiver by exploiting the transmission characteristics of twisted pair wire. A novel technique is proposed in this thesis to reduce common-mode noise coupled into the differential mode signal of a twisted pair cable, by adding an identical but inverted version of the common mode signal component. The resulting signal is the differential mode signal without the common mode RFI noise. Simulations using Matlab shows that this technique can reduce RFI by as much as 38.7 dB.

Acknowledgement

First of all, I would like to express my gratitude and appreciation to my supervisor, Dr. Tet H. Yeap. His guidance and support was the driving force behind the successful completion of my thesis work. Special thanks to Mr. David Fenton for his help with modeling, and to Bell Canada for supporting this research. Thanks to my colleagues in Nortel Networks for providing characterization data of the existing copper loop plant and RFI susceptibility.

Table of Contents

List of Tables

Table of Figures

List of Acronyms

AC	Alternating Current
ADC	Analog to Digital Converter
ADSL	Asymmetric Digital Subscriber Loop
AGC	Automatic Gain Control
AM	Amplitude Modulation
ANS	Adaptive Noise Suppression
AWG	American Wire Gauge
AWGN	Additive White Gaussian Noise
BER	Bit Error Rate
BT	Bridge Tap
CAT-3	Category 3 unshielded twisted pair cable (voice grade)
CM	Common Mode
CO	Central Office
CPE	Customer Premises Equipment
CRTC	Canadian Radio and Tele-Communications agency
CW	Constant Wave
DAC	Digital to Analog Converter
DM	Differential Mode
DMT	Discreet Multi-Tone modulation
DSL	Digital Subscriber Loop
DWMT	Discreet Wavelet Multi-Tone modulation
EM	Electromagnetic
EMC	Electro-Magnetic Compatibility
EMF	Electromagnetic Field
FEXT	Far-End Cross-Talk
FFT	Fast Fourier Transform
FIR	Finite Impulse Response digital filter
FTTC	Fiber To The Curb
FTTH	Fiber To The Home
HAM	Amateur radio
IFFT	Inverse Fast Fourier Transform

IIR	Infinite Impulse Response digital filter
JWI	Juncture Wire Interface
LBC	Loop Balance Correction
MPEG-2	Motion Picture Group video compression standard 2
NEXT	Near-End Cross-Talk
PIC	Plastic Insulated Cable
PSD	Power Spectral Density
PVC	PolyVinyl Chloride (plastic)
QAM	Quadrature Amplitude Modulation
QOS	Quality Of Service
RF	Radio Frequency
RFI	Radio Frequency Interference
SIR	Signal to Interference Ratio
SNR	Signal to Noise Ratio
SSB	Single Side-Band
UTP	Unshielded Twisted Pair cable
VCO	Voltage Controlled Oscillator
VDSL	Very-high speed Digital Subscriber Loop
xDSL	any non-standard DSL

1 Introduction

Recent deregulation of the telecommunication market and increasing popularity of the Internet has pressed traditional telephone companies and new telecom service providers to increase the bandwidth available to customers.

The progressive deregulation of the telecommunication market has forced the well-established operating companies in Canada and the USA to restructure to provide new services as profit margins dwindle in the long-distance market due to increasing competition. Deregulation is a two edged sword, it allows unregulated competition in the telecom market as well as any carrier to offer any type service such as voice, data, and video. As time progresses telecommunications users will have the option of receiving their telephone, Internet and television services through twisted pair, coax cable or microwave and satellite.

One important source of revenue for telephone operating companies today is the Internet. In fact the Internet is the main driver for Digital Subscriber Loop (DSL) technology today. The minimum bandwidth requirement for each type of service is also a technology driver for DSL. For example, the bandwidth required for Internet access can vary from 14.4 kbps to several Mbps. Conversely, to provide MPEG-2 video a minimum bandwidth of 26 Mbps is required. To be fully marketable, DSL modems will be required to provide a bandwidth high enough to provide full motion video such as MPEG-2.

One impediment to the delivery of high-speed access is the loop plant. Unfortunately, the most popular type of twisted pair cable is category-3 (CAT-3) cable which is severely limited in bandwidth due to it's high attenuation at high frequencies [1]. Upgrading the loop plant with high capacity transmission lines such as fiber, in Fiber To The Home (FTTH) or Fiber To The Curb (FTTC) configurations, is not a palatable alternative since loop plant is a major capital cost for operators. In addition, well up too 90% of installation costs are civil costs. For example, Bell Ontario alone has over ≈9 Billion dollars worth of installed copper

loop plant. Fiber will slowly penetrate into the existing loop plant as it ages and requires replacement, but this is a slow process and many decades will pass before the entire plant is converted to fiber optics.

The limited bandwidth available on twisted pair cable can be surmounted by clever coding techniques such as Quadrature Amplitude Modulation (QAM), Descreet Multi-Tone modulation (DMT), Discreet Wavelet Multi-Tone modulation (DWMT) and others. The tradeoff of using such techniques is the increased Signal to Noise Ratio (SNR) required from the channel for a given Bit Error Rate (BER). In addition to the limited bandwidth, Unshielded Twisted Pair (UTP) cable is not very resistant to external noise sources at frequencies above voice. In essence the usable bandwidth of UTP cable is below 2 MHz in which low frequency HAM bands and AM radio are located, creating substantial RFI sources in the DSL transmission band.

1.1 *Motivation for this Thesis*

Twisted pair cable is a poor transmission line at frequencies above voice. In addition to suffering from high loss, twisted pair is susceptible to high levels of RFI ingress causing less than optimal SNR. Adequate SNR is crucial for high-bit-density modulation techniques such as QAM and DMT. A method to reduce noise on twisted pair would be a major benefit to DSL technology. Leveraging of DSL technology can be achieved through the integration of a noise reduction scheme into a DSL modem product. The additional SNR gained by the noise filter will allow extended loop length or additional bandwidth, compared to a similar product without a noise suppression scheme.

Noise mitigation is one of the keys in providing affordable high bit rate access to the Internet and future digital services for residential and small business customers.

1.2 Thesis Objective

The objective of this thesis is to develop a method of reducing common mode interference in the differential transmission path of twisted pair cable, with particular emphasis on RFI noise.

1.3 Organization of this Document

This document is organized into five main sections. This section is the Introduction and is followed by a Background and Literature Review. The third section is a detailed description of the Adaptive Noise Suppression technique. Simulation results are presented in section four: Simulation and Prototype Results. Finally, conclusions on the adaptive noise suppression technique is presented in the Summary and Future Work section.

1.4 Main Contributions

A method of reducing interference in communications channels and is especially, but not exclusively, applicable to suppression of common mode noise, including radio frequency interference in digital subscriber loops of telephone systems.

2 Background and Literature

2.1 Two-wire Transmission Lines and Twisted Pair wire

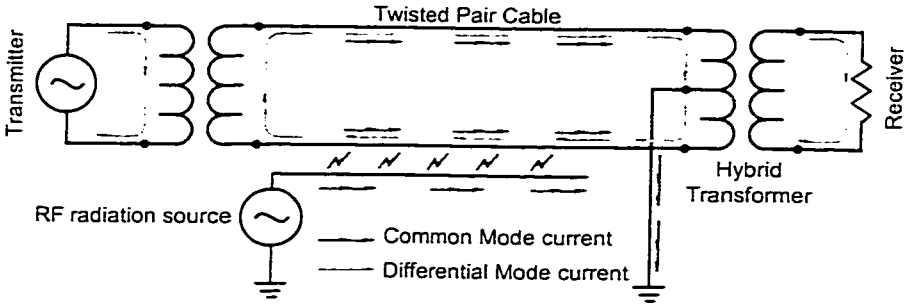

Figure 2.1: Twisted Pair Wire Transmission Modes

A two wire transmission line inherently contains two transmission modes: A differential mode (DM) for which electromagnetic waves (signal) travel between the two conductors of the two-wire transmission line, regardless of it being straight wire or twisted. And secondly, a common transmission mode (CM) where signals travel between the wire pair and earth or any other common ground.

2.1.1 Differential Mode

DSL modems, as with POTS, use the differential transmission mode of a copper loop as seen in Figure 2.1. In this mode, current flows in opposite directions on the two conductors at any cross-sectional point along the copper loop. Voltage is distributed equally between the two conductors with respect to ground. Given loop voltage X, conductor A and B will each have ½X volts respectively, when the conductor voltage is measured with reference to ground.

This is the preferred transmission mode since it is not affected by external RF radiation sources, assuming that the loop is perfectly balanced.

Balance refers to the matching of the distributed impedance of each loop conductor with respect to ground. Therefore, perfect balance can only be achieved if both loop conductors exhibit the same impedance with respect to ground. Under such conditions the common mode current on each of the loop wires are equal and will cancel in the hybrid transformer of the receiver as shown in

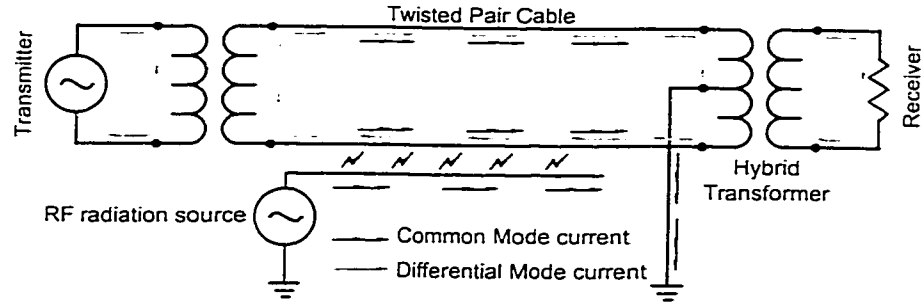

Figure 2.1.

Unfortunately, a completely balanced loop is difficult if not impossible to achieve. As a result of the balance limitation, a copper loop is susceptible to noise pickup through conversion of common mode signals into the differential transmission mode.

2.1.2 Common Mode

Signals generated in common mode on the loop are products of the loop configuration, local environment and proximity to RFI and impulse noise generators. All three factors contribute to the amplitude of the common mode signal seen on any given loop. Under severe conditions common mode signals can attain levels of 0 dBm in real loop plant as discussed in 2.1.4.3 and 2.1.4.4.

Since the CM of a loop acts as a dipole antenna [13], the physical configuration of the copper loop such as length, number of loop sections, number of adjacent pairs and shielding will establish the gain of the antenna created by the loop. Figure 2.3 is an example of a typical distribution and drop configuration for aerial and buried installations.

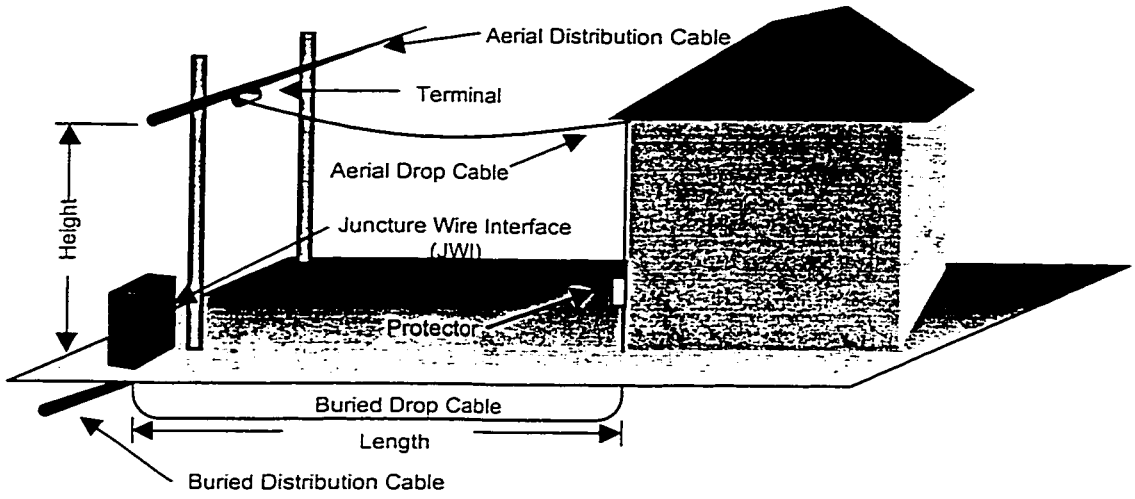

Figure 2.3 Typical Residential Aerial/Buried Drop Configuration

As well the environment can influence the amount of RF energy coupled onto the loop, for example the ambient field strength of a RF signal at the loop decreases if the cable is buried compared with a similar aerial installation. The proximity of metallic objects to the loop can also locally influence the field strength of a given RF signal, since these objects can act as passive radiators. Finally, the orientation of the loop with respect to the RF source will provide the coupling level of the EM field to the loop and thus the CM signal level, generated by this field. See Figure 2.5

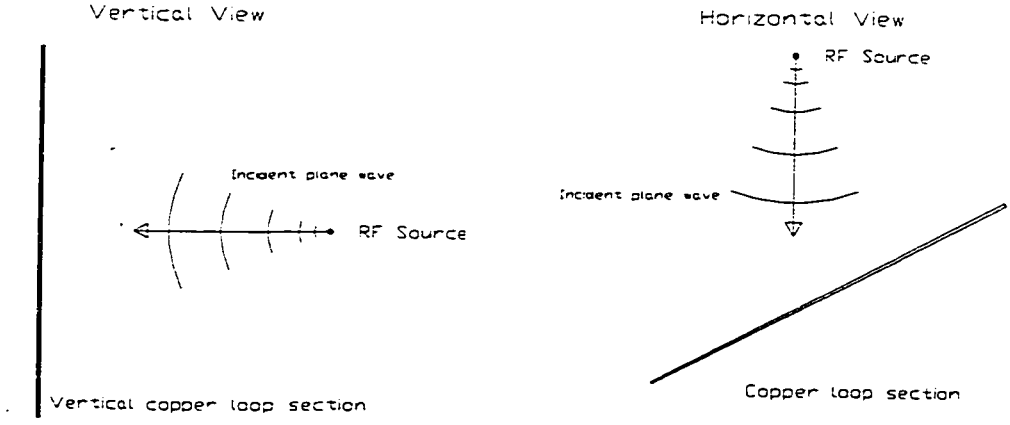

Figure 2.5 EM Coupling Level vs. Loop Orientation

In Figure 2.5 maximum coupling occurs when the direction of propagation of an incident plane wave is perpendicular to the wire. For the vertical case if we consider the directional radiation pattern of a vertical dipole antenna seen in Figure 2.7, the far field electrical and magnetic fields are given by the following equations [2]:

$$H_\phi = j\frac{Idl}{4\pi}\left(\frac{e^{-j\beta R}}{R}\right)\beta\sin\theta, \quad \text{A/m}$$
$$E_\theta = j\frac{Idl}{4\pi}\left(\frac{e^{-j\beta R}}{R}\right)\eta_o\beta\sin\theta, \quad \text{V/m} \qquad (2.1)$$

where:

I = Current in antenna

l= length of antenna

$\beta = 2\pi/\lambda$

R = Distance from antenna

θ= Angle of elevation from horizontal plane see Figure 2.7

$\eta_o \cong 120\pi\ (\Omega)$.

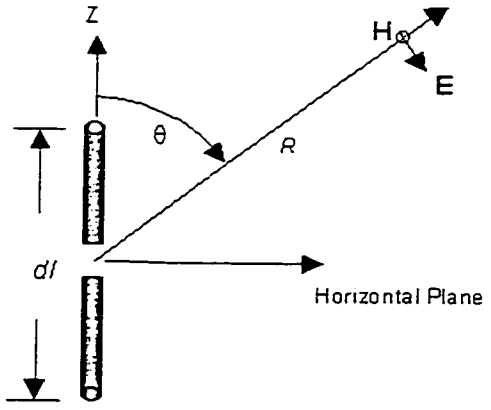

Figure 2.7 Vertical Dipole

From equation 2.1, the maximum coupling occurs when θ is equal to 90°. It can be shown that both the impedance and directional pattern of an isolated antenna is identical in both transmitting and receiving modes [2][3]. Therefore, maximum coupling for reception of a RF signal will also occur at a perpendicular angle to the vertical section of copper loop. It is important to note that if earth is considered a perfect conducting plane, then the vertical loop segment will have a mirror image below ground. Thus, only half of the wire length is required for a given wavelength. For example, a quarter wavelength ($\lambda/4$) of vertical wire is equivalent to a half-wave dipole ($\lambda/2$) antenna in free space.

Horizontal loop sections have a more complex radiation patterns since the horizontally suspended wire acts no longer as a simple dipole in free space, but rather as a two-element antenna array due to the proximity of the ground plane. Figure 2.9 shows the typical configuration of the antenna array created by a suspended wire parallel to a conducting plane. Unfortunately, the computation of the **H** and **E** field for this case becomes complex since the radiation pattern is not only dependent on the effective wavelength of the antenna but also the geometry of the array and the amplitude and phases of excitation of each element. A complete dissertation on this subject can be found in [2]. If a broadside array is assumed for all suspended loop cases, where maximum coupling occurs at a 90° angle to the length of the wire, a good empirical model can be developed to estimate RFI coupling on to twisted pair cable from external RF sources. An estimation of the DM RFI noise level can be computed to within 5 dBm of the actual measured DM power induced by RFI source in the AM band. Such an empirical model uses transmitter power, Latitude and Longitude coordinates as parameters to compute the electrical field strength and incident angle of the radio wave with respect to the copper loop, and loop balance. Only these parameters are used to determine expected CM and DM RFI levels in a given loop, with the assumption that the horizontal loop section as an antenna with a gain of 1 [4]. Thus, it is possible to apply a generalization with respect to CM coupling for horizontal loop sections

without significant loss of accuracy, given that the model developed in [4] is simplistic.

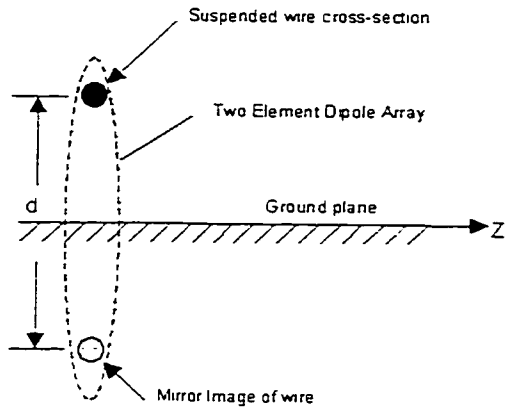

Figure 2.9 Antenna Array Generated by a Conducting Plane

The final parameters influencing the CM signal level on a loop is the proximity of that loop to the RFI or impulse noise source and the polarization of the interfering signal.

2.1.3 Balance

The degree of signal conversion from one transmission mode to the alternate transmission mode is measured as a ratio of signal voltages and is defined as follows: Longitudinal balance is defined as the ratio of common mode noise voltage to the differential noise voltage produced by it.

$$Longitudinal\ Balance = 20 \cdot Log_{10}\left|\frac{V_{CM}}{V_{DM}}\right| \quad dB, \quad (2.2)$$

where V_{CM} is the total longitudinal source voltage and V_{DM} is the resulting metallic voltage appearing across the load. Longitudinal balance is usually thought of as being a function of the differences of impedances to ground of the transmission line. This measurement gives the effective longitudinal balance.

2.1.3.1 Capacitive & Inductive Coupling Models

Miller [5] has proposed a general loop model that includes loop imbalance around earth ground and signal coupling between two loop pairs. His work is mentioned here for reference purposes only, since this work will directly use balance figures to perform CM signal leakage into DM.

Most twisted pair models use RLGC parameters (see section 4.1.3) measured from physical cable, or curve fitting algorithms when sparse measurement data is available [6]. Two wire transmission line models, without wire twisting, is used since it provides accurate results given accurate measurement data and developing a model that includes loop wire twisting is a complex mathematical exercise. There are definite benefits to wire twisting as described below.

Twisting two wire transmission lines such as copper loop pairs provides a twofold benefit. First, electromagnetic interference can be minimized by the fact that if wires alternate in an electromagnetic field (EMF) the net current and voltage induced on the wires will be zero (see Figure 2.11). It must be specified that the effectiveness of EMF cancellation is inversely proportional to the twist length with respect to the wavelength of the EMF. In other words, as the twist length becomes shorter the twisted pair will exhibit improved crosstalk immunity at higher frequency. In addition, a slight variation in twist length for each adjacent loop pairs will further minimize crosstalk in a cable [7]. Thus a twisted pair cable can be optimized to reduce crosstalk within the frequency range of interest for xDSL.

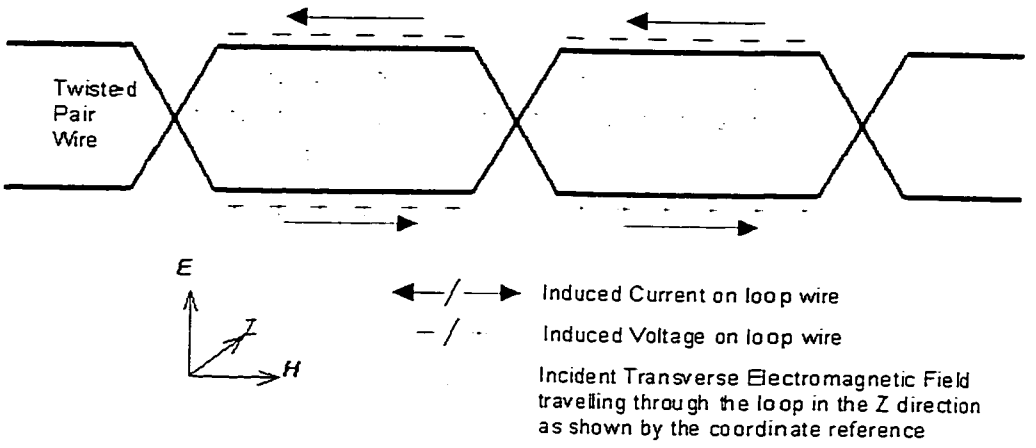

Figure 2.11 Effect of Twisting Two Wire Transmission Lines

The second benefit of twisting is to improve capacitive loop balance with respect to shield (ground), and adjacent pairs in the twisted pair cable.

2.1.3.2 RFI Coupling Model

Typical RFI coupling models are based on empirical formulas due to the complexity of modeling RF wave propagation and CM coupling onto irregular loop plant "antennas" and the unpredictability of cable placement with respect to reflective structures. The empirical formulas presented in T1E1 [6] are fairly accurate despite very general assumptions. In specific situations a correction factor can be applied to increase prediction accuracy of such formulas. In addition to sources such as T1E1 telecommunications standards [6], the author was involved with a study to fine-tune one such empirical formulas to increase prediction accuracy in the AM frequency band, which resulted in the following equation:

$$P_{DM} = 10\log P_{kW} + 20\log\frac{300}{D_{km}\cdot B} - 50.92 \text{ (dBm)}, \quad (2.3)$$

where P_{DM} is the differential RFI signal level resulting from the coupling of the RFI source to the cable. P_{km} is the AM transmitter power level in kilo-watts and D_{km} is

the distance between the transmitter antenna and the twisted pair cable. *B* is the cable balance.

In addition to equation 2.3, but not discussed here for reasons of intellectual property, an extra factor was added to the formula to correct the coupled signal level for cable orientation in the electromagnetic field generated by the RF source.

2.1.4 Copper Loop Plant Basics

2.1.4.1 RFI Frequency Bands in xDSL Bandwidth

The known frequency bands where potential RFI could interfere with DSL modems such as ADSL, XDSL and VDSL, are as follows:

AM Radio frequency band with transmitter frequencies ranging from 535 kHz to 1605 kHz centered at 10 kHz intervals. These transmitters use amplitude modulation with carrier wave output power ranging from 100 Watts to 50 kW[1]. Signal transmission originates from fixed antenna sites located in or near larger population centers. As well, AM radio stations usually use different radiation patterns and transmit power for day/night operation.

Amateur (HAM) Radio operators can transmit in the following RF bands: 1.81 MHz to 2.0 MHz, 3.5 MHz to 4 MHz, 7.0 to 7.3 MHz, and 10.1 to 10.15 MHz. HAM operators have the choice of transmitting Continuous Wave (CW) or AM with a transmitter power limit of 1000 Watts, or Single Side Band (SSB) with a maximum instantaneous envelope power of 2200Watts[1]. Signal transmission can originate from any location including mobile transmitters for shorter wavelengths. The CRTC does require an antenna site location from HAM operators in the form of a postal code, but regulations are not strictly enforced and the operator is left to

[1] CRTC limits in Canada. Specifications subject to change in different countries.

his own devices. Radiation patterns from HAM antennae can vary greatly from dipoles to high gain directional antennas. As well HAM operators can frequency hop in relatively short time intervals, which can be as short as a few seconds.

In addition to AM and HAM frequency bands, the spectrum from 9 kHz to 10 MHz is allocated to services such as commercial short-wave, Aviation communications and radio locator beacons, Maritime navigation and communications, Standard time signals and other services [8].

Since the frequency spectrum from 9 kHz to 10 MHz is fully allocated to radio communications, DSL modems must possibly cope with the presence of RFI noise anywhere in its communication bandwidth. In addition, DSL modems must not radiate RF energy as to affect essential services such as aviation beacons. As a result DSL modems are prohibited from overpowering RFI by increasing the transmitter output power. Again, limited loop balance causes a portion of the DSL signal energy to be radiated from the copper loop through the common mode transmission path.

2.1.4.2 Typical Loop Plant Structure and Characteristics

Typical telephone loop plant is composed of three sections each with distinctive characteristics, which influences DSL deployment strategies. From the Central Office (CO) towards the Customer Premises Equipment (CPE) the copper loop is composed of a feeder section, distribution section and drop cable. Each section is interconnected to the following section through a cross-connect device such as a Juncture wire Interface (JWI)[2] for Feeder to Distribution cable interconnect, or a

[2] The terminology is dependent on the operating company. This document uses Bell Canada's loop plant terminology.

distribution terminal to connect drop cables to a distribution cable as depicted in Figure 2.13.

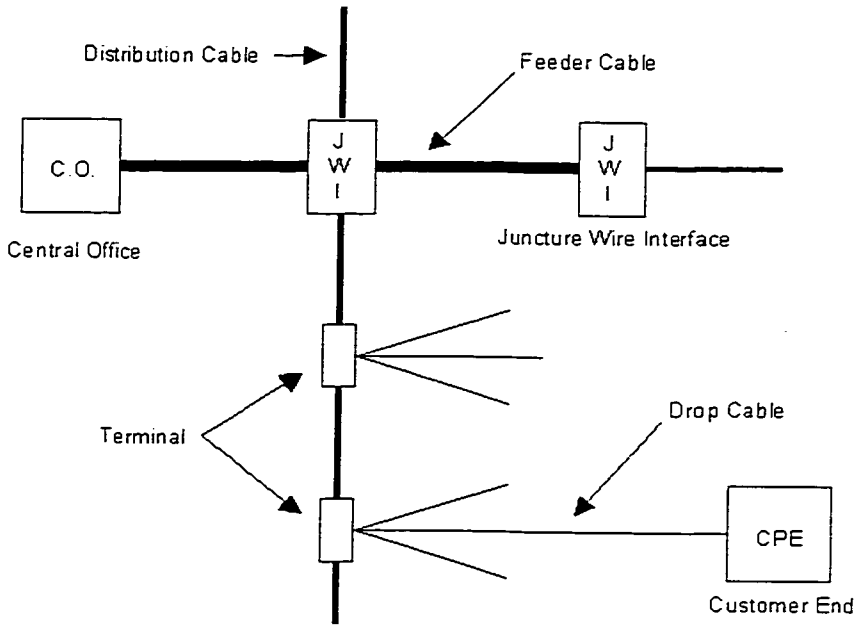

Figure 2.13: Typical Outside Plant Configuration

Feeder cable can contain anywhere from 25 to as many as 4,200 wire pairs bundled in 25 pair groups using standard color coding schemes. All modern feeder cable types are constructed with a copper or aluminum shield jacketed with HD polyethylene, HMW polyethylene, or Vinyl. Cables may also contain steel armor for severe-duty applications.[9]

Aerial feeder cable is supported with an external messenger wire (or supporting strand) or can be manufactured with the supporting strand integrated inside the cable jacket. Aerial cables are usually Plastic Insulated Cable (PIC) cables, where individual wires are insulated with Polyethylene, Polypropylene, dual expanded polyethylene, or PVC. Although less popular, air core (pressurized) pulp cable may also be used in aerial applications. In addition to regular PIC cable, feeder cable can be filled with water displacing gel.

Buried cables are available as pressurized air core pulp insulated or gel filled cable.

Feeder cable can contain 19, 22, 24, or 26 (AWG) wire gauge sizes. High pair count feeder cable will usually contain 24 or 26 AWG wire.

Distribution cable construction is similar to feeder cable, except that the pair count in the cable is lower. The distribution section of the cable plant is characterized with terminal connection equipment splicing the distribution cable at periodic intervals along the length of the cable. A standard practice used by telephone operating companies is splicing into the distribution cable without cutting the unused wire pair continuing past the terminal access point. The excess wire connected to the loop is referred to as a bridge tap. Bridge taps (BT) normally don't impact regular POTS service since the resonant frequencies of this transmission line stub are above voice frequency. Unfortunately for DSL type services, the resonance created by the BT will severely impact the usable frequency bandwidth of the DSL modems. The location in the loop, length and number of bridge taps will determine the frequencies at which the differential signal will be attenuated and possibly phase distorted. Fortunately, there exists standards on the possible configurations of bridge taps for twisted pair loops.[10]

The last component of the local telephone distribution plant (outside plant) is the Drop cable. Drop cable types can vary from single pair flat (untwisted) cable to multi-pair, or even shielded cable. Drops are usually short in length since they are located between the distribution right of way, such as a street or back-lot, and the customer's home.

2.1.4.3 RFI levels reported in T1E1 standards

The VDSL system requirements document [19], specifies three noise threat scenarios based on previous T1E1 technical contributions on RFI threat evaluations for ADSL and VDSL. Table 1 lists these three threat scenarios for the AM frequency band. In addition, the requirements document specifies a DM signal level of −10 dBm for Amateur Radio noise sources.

Table 1: Three AM Radio Noise Threats for VDSL.

	Model 1 (high-density urban with co-located transmitters)		**Model 2** (high-density urban with primary/secondary transmitters)		**Model3** (suburban)	
Frequency (kHz)	**CM** dBm (50Ω)	**DM** dBm (100Ω)	**CM** dBm (50Ω)	**DM** dBm (100Ω)	**CM** dBm (50Ω)	**DM** dBm (100Ω)
660	0	-60	5	-55	0	-60
710	30	-30	10	-50	10	-50
770	-10	-70	0	-60	-10	-70
1050	5	-55	10	-50	5	-55
1130	30	-30	30	-30	10	-50
1190	0	-60	0	-60	0	-60
1280	5	-55	5	-55	5	-55
1330	0	-60	5	-55	5	-55
1480	-10	-70	-10	-70	-10	-70
1600	0	-60	0	-60	0	-60

2.1.4.4 RFI Test Results from Bell Canada Access Plant

This particular study focused on drop cables, being the last section of the distribution plant closest to the DSL receiver and is generally unshielded. Feeder and distribution cable do contribute to RFI coupling into the DM to a lesser extent than drop cables since these cable types are shielded. As well, in high pair count cables extra shielding is gained by the high number of adjacent loop pairs. Conversely, the high loop pair density will cause other types of signal impairments such as Far end (FEXT) and near end (NEXT) crosstalk.

A large number of drop cable types are or were available commercially, are in use today in copper loop plants. The number of drop cable types deployed in any given

local access network will depend on the age of this network and the modernization commitments of the operating company. The author has seen operational cable plants that use every type of standard cable from modern multi-pair category 3 drop cables with a glass strength member to cotton braided twin axial cable (untwisted) deployed from wooden terminal boxes. The RFI immunity of these cables differs greatly as a result of different construction methods and configurations.

As shown in Figure 2.15, different types of drop cable can affect the levels of DM RFI ingress by as much as 29 dB.[11] The levels shown for each drop type, is the compiled average of all test sites located in Repentigny Quebec for residential installations. The RFI sources used to measure the DM ingress are 8 AM radio stations located in the Montreal area and are listed as follows:

600 kHz – CIQC
690 kHz – CBF
730 kHz – CKAC
800 kHz – CJAD
850 kHz – CKVL
940 kHz – CBM
990 kHz – CKIS
1410 kHz – CFMB

Figure 2.17 shows the changes in DM RFI ingress levels as an average of all residential test sites located in Ottawa. With different drop types the DM RFI levels can change as much as 29.9 dB. The RFI sources used to measure the DM ingress are 4 AM radio stations located in the Ottawa area and are listed as follows:

580 kHz – CFRA
1150 kHz – CJRC
1200 kHz – CFGO
1310 kHz – CIWW

The drop cables used in Nortel's RFI field measurements are abbreviated as follows in Figure 2.15 and Figure 2.17:

Aerial 1 pr.: aerial 1 pair flat drop (NORTEL #22309060)
Aerial 2 pr.: aerial 2 pair 6" twist length (NORTEL #22302005)
Aerial 6 pr.: aerial 6 pair 6" twist length (NORTEL #22221200)
Super PIC: 3 pair polyolefin insulated cable CAT 5 grade twist (Nordex/CDT)
Stand. Bur. Drop: Standard buried drop (NORTEL #22207030)
Stand. Bur. Drop w/ splice: Standard buried drop with splice at 25 meters
Shld Drop (no grnd): ungrounded Shielded drop
Shld Drop (grnd at terminal): Shielded drop grounded at terminal
Shld Drop (grnd at both ends): Shielded drop grounded at terminal and protector block

The measurements on the Drop cables were conducted in isolation of the loop plant. All test cables were placed in the same location as the existing drop cable. For buried cable the test cables were simply laid on the ground following the same route as the buried drop.

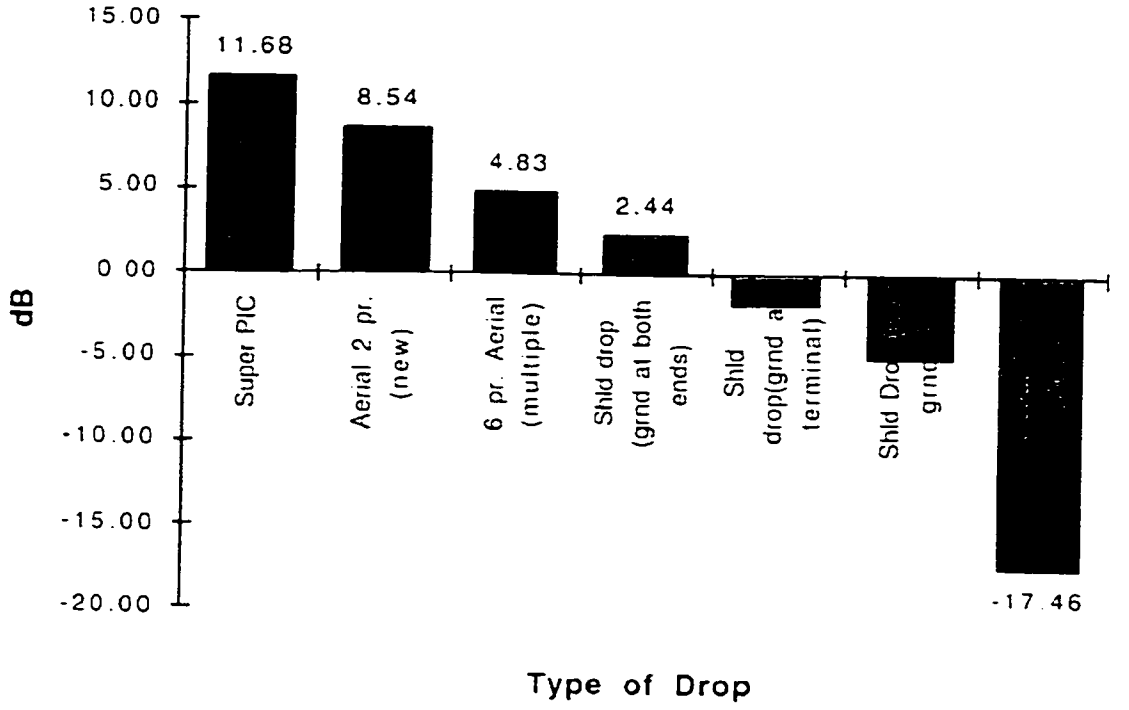

Figure 2.15: Reduction of RFI Levels over Existing Drop cables (Montreal)

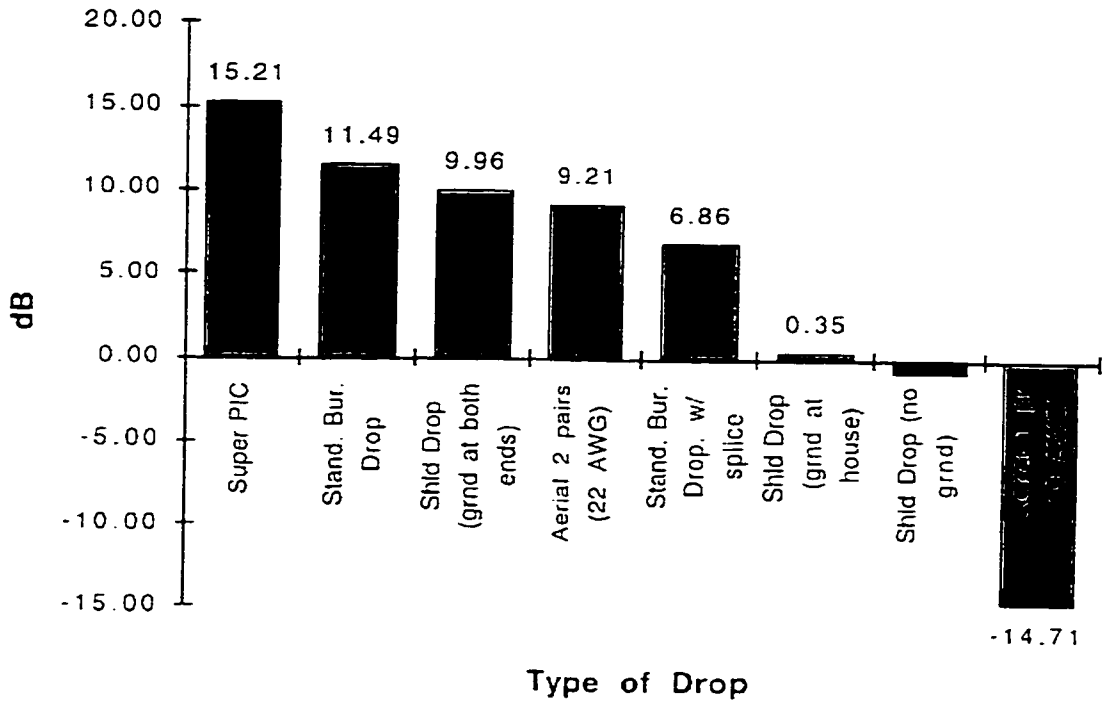

Figure 2.17: Reduction of RFI Levels over Existing Drop cables (Ottawa)

2.1.4.5 Recommended Transmit Signal Levels for DSL

Regulatory EMC limits for radio frequency emissions for communication devices imposes a limit on the level of radiation emitted by DSL modems such that this device does not interfere with licensed users of the same radio spectrum. The proposed power spectral density (PSD) limit of –60 dBm/Hz would meet emission limits in most countries if a worst-case loop balance of 30 dB were assumed. Unfortunately, amateur radio equipment sensitivity might impose a lower PSD to avoid generating signal egress levels that would interfere with receiving equipment [12].

2.2 *Existing Noise Mitigation Techniques*

Many different methods exist and are currently used to mitigate noise on twisted pair wire in telecom application and in other areas. Each technique has a niche application for which it is best suited, unfortunately these noise suppression methods have limitations that prevent successful integration into xDSL technology. A survey of these techniques have been included in this document as a basis for the following discussions on proposed (new) techniques as well as the Adaptive Noise Suppression technique, which is the main contribution of this thesis.

A well-known technique to suppress CM RFI in telecommunication equipment of any type, which use twisted pair wire, is the use of RF chokes or common-mode inductors. The RF choke is a transformer with a 1:1 winding ratio configured as shown in Figure 2.19, such that the mutual inductance of the coupled inductors creates very high impedance at RF frequencies when the device is excited with CM signals.

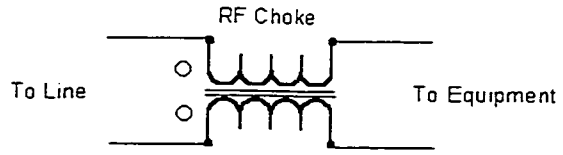

Figure 2.19 Common-mode (RF) Choke

Shielding twisted pair loops can decrease RFI susceptibility of the transmission channel with variable results. Proper grounding techniques are required to achieve improvement in RFI levels.

A related method to mitigate common-mode noise on a shielded twisted pair cable embodied in US patent no.: 3,705,365 dated Dec. 5, 1972 uses the shield wire as a common mode signal source combined with a three winding transformer wired in a common mode configuration. This technique consists of canceling the common mode signal on twisted pair by using the CM signal from the shield wire as the input to the third winding of the transformer. The transformer is configured to

generate a signal identical to the common mode signal on the twisted pair, but with opposite polarity to cancel the CM signal appearing on the differential pair (see Figure 2.21).

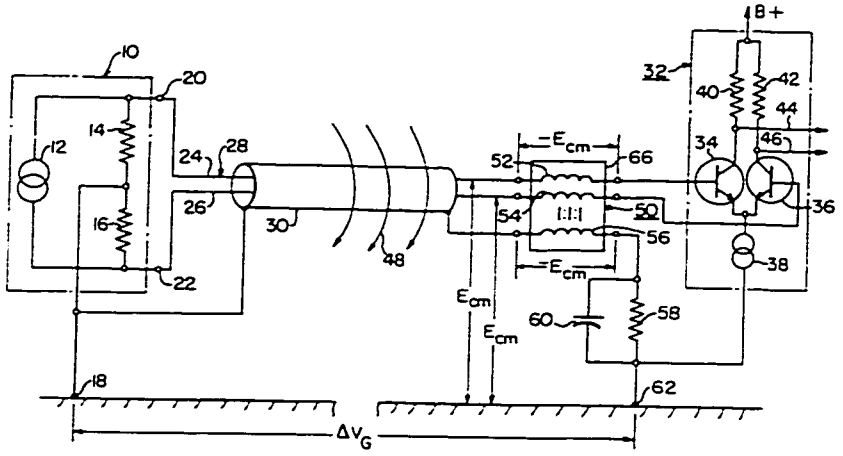

Figure 2.21: Common Mode Noise Cancellation system (US Patent 3,705,365).

In U.S. patent No.: 3,932,713, an induction cancellation circuit is used to minimize the effects of AC-induced signals on a telephone wire pair. The proposed circuit consists of a detector to detect on/off hook states on long loops subjected to high AC induction noise. An induction circuit is then used to cancel low-frequency AC noise on the line.

Analog and Digital Notch filters can also be used to notch the received signal (DM) where high RFI is present. Analog notch filters are usually fixed or expensive if adaptive. These filters are well suited to prevent saturation of Analog to Digital Converter (ADC) from high-level ingress noise. Conversely, digital filters are easily implemented and are readily adaptable. Given that such filters are located after the ADC in the signal chain, they cannot prevent saturation of the converter. As well, notching out the disturbing RFI noise from the message signal also degrades this signal by suppressing part of its transmission bandwidth, such that the overall benefit of eliminating the RFI signal is diminished.

2.3 Proposed Noise Reduction Techniques

One passive technique proposed by R.A. Combellack is an enhancement to the common-mode choke technique, where multiple RF choke transformers are distributed over the loop to suppress CM RFI and Crosstalk [13]. The total loop length can be shortened into smaller independent segments by creating high impedance barriers on the CM transmission mode. As a result the effective antenna length or resonance of the twisted pair loop is changed, as well less CM signal will propagate to the input of the receiving equipment reducing any CM to DM signal conversion due to equipment AFE imbalances. In addition to the CM chokes, Combellack also proposes a termination circuit presenting low impedance to ground for common-mode signals. Terminating CM transmission modes with half of its characteristic impedance minimizes CM to DM conversion of RFI and Crosstalk noise due to loop unbalance [13]. Unfortunately this technique does not attenuate CM signals converted into DM noise.

A modulation technique developed by Amati Communication Corp. called Discrete Multi-Tone (DMT) modulation and the variant Synchronous DMT (SDMT), are well suited for RFI prone communication channels [14]. DMT was developed to increase the maximum transmissible symbol rate on noisy communication channels with severe high frequency attenuation. DMT is a technique using FFT and IFFT in a filter bank configuration such that the serial data stream to be transmitted is distributed over n sub-channels before transmission. The reverse operation is performed at the receiver to recover the original serial data.

DMT confronts RFI noise by redistribution of the data stream from affected channels to other channels in its usable bandwidth, effectively silencing channels masked by RFI. As a result, the maximum transmission bit rate of the DSL modem must be reduced due to the loss of transmission channels from interference.

2.4 *Limitations of Existing and Proposed Noise Reduction Techniques*

Since existing and proposed techniques reviewed here have limitations that limit their applicability to DSL technology, a new technique is required to meet the noise requirements of ADSL, VDSL and other variants such that sufficient reach and data rates can be achieved through existing loop plant.

3 Adaptive Noise Suppression

The initial orientation of this research, to reduce noise on twisted pair as a method of conditioning telephone cable plant for use with high bit rate DSL technology, consisted of modifying loop balance to improve noise immunity. Unfortunately, Loop Balance Correction (LBC) proved to have limitations that would prevent a successful and cost effective implementation. Loop balance correction, which is an impedance correction technique, will be briefly discussed. Faced with a sub-optimal solution, a search for an alternative technique that would surmount the inadequacies of LBC was undertaken. Adaptive Noise Suppression is the result of the research into noise reduction on twisted pair loops.

Adaptive Noise Suppression is a novel technique to minimize noise on twisted pair transmission lines. ANS overcomes the limitations and problems faced by impedance correction techniques. The basic concept as well as the architecture of the ANS system for a single channel will be described. The intricacies of expanding the single channel to a multi-channel system will then be discussed. Finally a brief on possible implementations of ANS will be presented.

3.1 Loop Balance Correction

Initially a method for loop balance improvement was investigated, as it seemed a promising technique to reduce DM noise caused by CM signal and loop imbalance. Loop balance correction consists of generating a loop termination impedance which has a slight impedance imbalance such that the total impedance of each lead with respect to ground is equal. Therefore in theory, loop balance should improve.

Although changing the termination impedance of a twisted pair loop will affect balance, limitations due to reach, grounding and behavior over frequency reduces

the effectiveness of this technique. An impedance correction circuit will improve loop balance only on a limited loop distance from the apparatus, since the generated impedance is localized. Conversely, the loop impedance is distributed over the entire loop length. As such the loop imbalance may also be the result of a distributed impedance mismatch of the conductors with respect to ground.

The available ground reference used for the impedance correction network will have a substantial impact on the performance of the loop balance correction circuit. Considering that the termination impedance generated by the loop balance correction circuit is itself unbalanced with respect to ground and the loop leads, any signal or noise coupled into the ground reference will be directly injected into the DM. The level of the noise injected by the Loop Balance Circuit is dependent on the level of imbalance generated by the circuit, and is therefore proportional to the equivalent balance factor of the termination impedance.

Experimental tests were conducted in Repentigny Quebec residential drop cable with a simple impedance correction circuit, consisting of a variable resistor connected between both loop conductors and through a capacitor to ground (as shown in Figure 3.1). An example of balance improvement is shown in Figure 3.3 with different capacitance values.

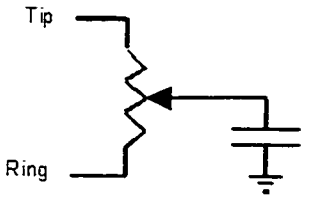

Figure 3.1: Loop Balance Correction test jig.

Longitudinal Balance test results (Figure 3.3) show that the balance improvement in narrow band in nature, and that improvements in one frequency range may cause a degradation in balance elsewhere in the frequency spectrum. Signal spikes in the longitudinal balance spectrum are caused by RF ingress from AM radio stations in the greater Montreal area coupling through the loop balance correction jig.

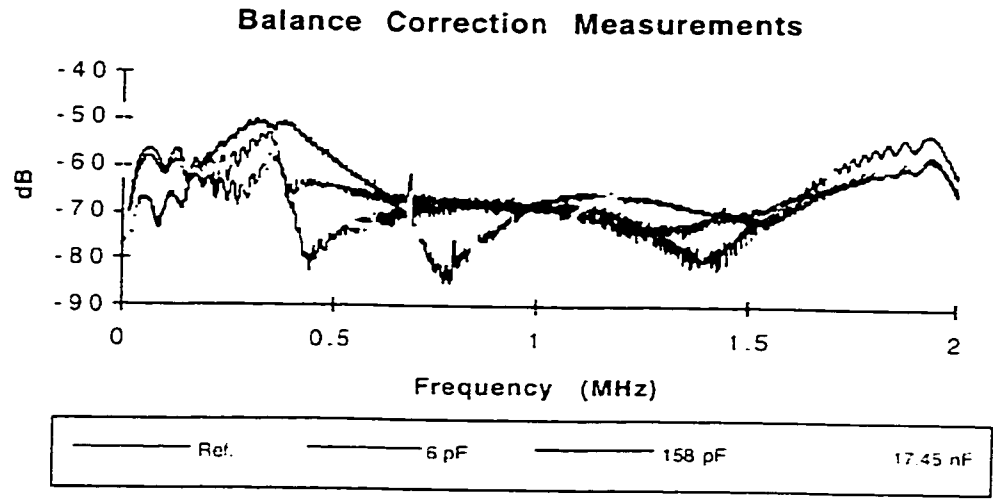

Figure 3.3: Balance response generated by Loop Balance Correction test circuit.

Assuming an ideal ground reference can be provided, adequate loop balance correction can only be achieved with a significantly more complex impedance generation circuit.

3.2 *Adaptive Noise Suppression*

Given the limitation of loop balance improvement techniques, the research focus changed to an alternative noise mitigation technique that would be independent of grounding, loop length and impedance. The alternative noise mitigation technique should also fully exploit the following twisted pair transmission media characteristics:

- The existence of two transmission modes, DM and CM.
- The signal coupling between the two transmission modes (longitudinal balance).
- Ingress of external RFI and impulse noise is coupled onto the CM.

- Due to loop balance characteristics, Noise levels on CM will always be larger in magnitude than DM noise.

As well, the noise mitigation apparatus should be self contained and integrate-able into DSL modem devices. The Adaptive Noise Suppression (ANS) technique presented below meets all design requirements stated here.

ANS is a novel application of, and extension to common noise and echo cancellation techniques used in audio applications. DM noise caused by ingress from RFI sources coupling into a digital subscriber loop can be eliminated if we consider that the RFI signal is present in both transmission modes CM and DM.

The premise behind the ANS concept is the fact that DM noise contributed from a CM source can be extracted (subtracted) from the DM, given that the CM signal source is highly correlated with the noise present in the DM. A mathematical proof for this concept follows:

$$
\begin{aligned}
\text{Let} \quad V_A &\equiv \text{The voltage on lead A w.r.t. Ground} \\
V_B &\equiv \text{The Voltage on lead B w.r.t. Ground} \\
V_S &\equiv \text{The differential signal from the transmitter} \\
V_{Noise} &\equiv \text{The Common - mode noise signal} \\
B &\equiv \text{The Logitudinal Balance Factor} \\
B &= \left(\frac{V_{DM} \text{ measured}}{V_{CM} \text{ injected}} \right) \\
V_S = V_A - V_B \quad &\text{and} \quad V_{Noise} = V_A + V_B
\end{aligned}
$$

The composite differential mode voltage is given by:

$$
\begin{aligned}
V_{DM} &= V_S + B \cdot V_{Noise} \\
V_{DM} &= (V_A - V_B) + B \cdot (V_A + V_B)
\end{aligned}
$$

Where as the common mode voltage is given by:

$$
\begin{aligned}
V_{CM} &= V_{Noise} + B \cdot V_S \\
V_{CM} &= (V_A + V_B) + B \cdot (V_A - V_B)
\end{aligned}
$$

Let the processed signal from the output of the ANS system equal the following equation:

$$V_{ANS} = V_{DM} - B \cdot V_{CM}$$
$$V_{ANS} = (V_S + B \cdot V_{Noise}) - B \cdot V_{CM}$$
$$V_{ANS} = (V_S + B \cdot V_{Noise}) - B \cdot (V_{Noise} + B \cdot V_S)$$
$$V_{ANS} = [(V_A - V_B) + B \cdot (V_A + V_B)] - B[(V_A + V_B) + B \cdot (V_A - V_B)]$$

Simplifying:

$$V_{ANS} = (V_A - V_B) - B^2 \cdot (V_A - V_B)$$

If $V_{CM} > V_{DM}$ and $B << 1$ then,

$$V_{ANS} \cong (V_A - V_B)$$
$$V_{ANS} \cong V_S,$$ and as a result the noise is suppressed.

For CM RFI to have a considerable effect on the DM signal, the CM noise source must have a significantly larger magnitude than the DM signal to overcome attenuation from cable balance as the RFI signal is converted from CM to DM. Therefore the '$V_{CM} > V_{DM}$' condition is satisfied since the CM reference signal is stronger. As well, a twisted pair copper loop is required to have a decent balance to be viable for data transmission. Assuming a worst case balance of at least 30dB (i.e.: B = 0.0316), the residual noise term ($B^2(V_A$-$V_B)$) has a magnitude equal to 0.1% of the recovered signal V_S.

3.3 *ANS Basic Concept*

The invention will reduce dominant longitudinal noise in the differential mode signal presented at the receiver loop interface (twisted pair or copper).

Although the previous equations describing the ANS concept look trivial, a practical implementation requires increased complexity to achieve signal suppression. The noise suppression system, in addition to performing RFI noise suppression on the DM signal, must also pre-process the reference (CM) signal to

compensate for loop loss, phase distortion, and prevent the introduction of additional noise into the DM as a result of ANS filtering activities.

The ANS technique reduces common-mode noise coupled into the differential mode signal of a twisted pair cable, by adding an identical but inverted version of the common mode signal component present in the differential mode signal extracted by the hybrid circuit. The resulting signal is the differential mode signal without the common mode noise component as it is suppressed by the phase inverted version of the common mode noise, introduced by the noise suppressing circuit. This is accomplished by extracting CM noise from the twisted pair loop and adding this signal, once inverted and magnitude adjusted, to the DM signal extracted by the Hybrid circuit. Figure 3.5 is a simplified block diagram of the ANS concept.

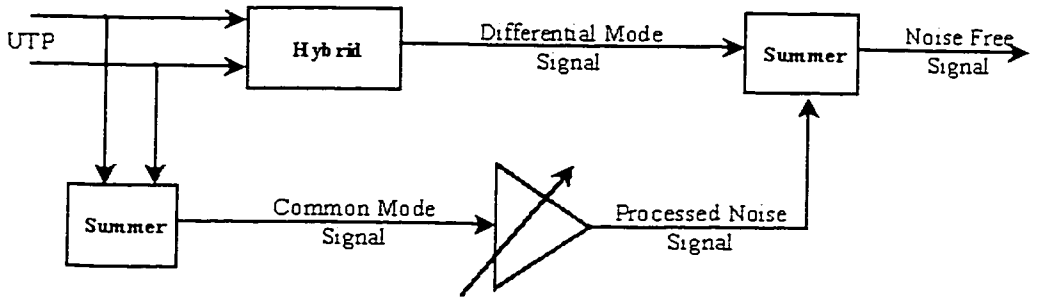

Figure 3.5: Adaptive Noise Suppressor Simplified Block Diagram

3.4 Architecture

3.4.1 Single Channel ANS System

The following is a detailed description and expansion on a practical ANS implementation, which functions with twisted pair transmission line characteristics.

The first requirement for noise suppression via signal cancellation is an effective method of extracting both common-mode and differential mode signal from the twisted pair media. The differential mode signal is always present in any telecommunication equipment since it is the normal transmission mode for twisted pair media. Common mode is usually not extracted (sensed) by DSL modem equipment considering it has no value as a communication channel. It does however provide a correlated noise estimation signal source to suppress RFI noise contained in the DM signal. Since it is necessary to properly extract the CM signal, careful attention is required in the design of the common mode extraction circuit.

A good measurement of the common mode signal that exists in an unbalanced twisted pair cable is crucial in the proposed design. For example, in one design (Amati design) common mode noise is estimated by measuring the voltage across the center tap of a hybrid transformer and the ground. The common mode noise estimation could be inaccurate because of poor ground reference. For example, this is especially true in rocky regions. In the proposed design, common mode noise is estimated by adding the in-phase tip signal and opposite phase ring signal with respect to an arbitrary but controlled ground reference. The DC offset between the twisted pair cable and the reference will have no effect on the ANS system since we are concerned only by the AC component of the signal. In fact an artificial ground reference can be used when an active circuit is used for CM detection as proposed. We note that the common mode signals, in both tip and ring portions of the cable are in phase with each other. Therefore, the common mode signal is extracted while the differential mode signal is canceled out by the addition of tip and ring signals at summer 7. See Figure 3.7.

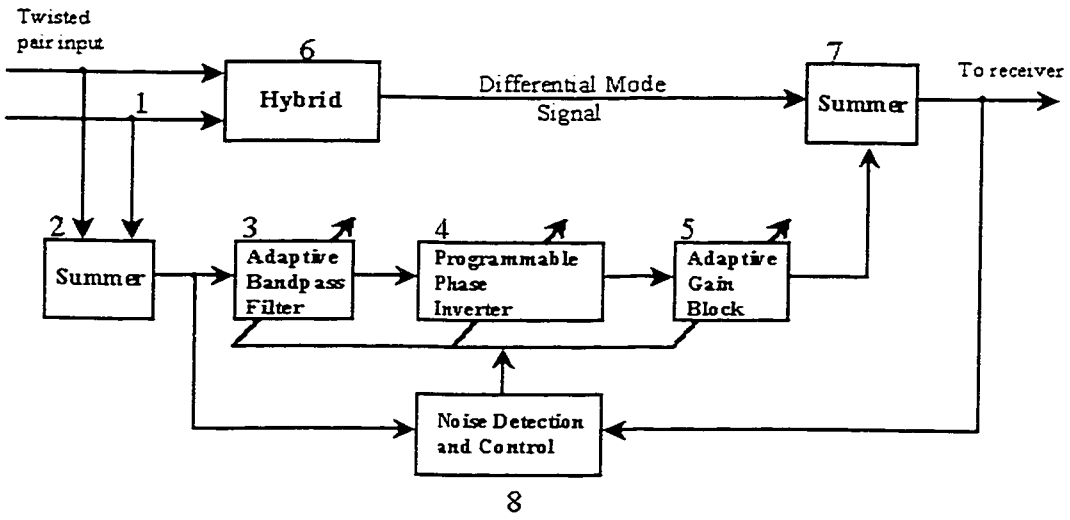

Figure 3.7: Block Diagram of a single channel ANS system.

Unfortunately, the CM reference signal present on the twisted pair media is related to, but not identical to the DM noise generated by these signals. The design of the ANS system must account for the differences between the reference signal and the noise signal to accomplish the goal of noise suppression.

As presented in section 2.0, the DM has a different propagation delay than the CM. As a result a phase delay exists between signals present on each transmission mode. The delay is arbitrary and dependent on the environmental conditions surrounding the twisted pair conductors, coupling mode of the noise signal and the receiver analog front end. A method of signal re-alignment is therefore required to permit signal cancellation between the noise estimate signal (CM RFI) and the RFI noise present in the DM.

Although arbitrary from loop to loop, there exists a phase relationship between the two propagation modes. Furthermore, this relationship is not constant over frequency. The magnitude of the difference in phase between the two propagation modes increases with frequency. Beyond a few MHz, multiple periods of phase delay is exhibited between the common and differential modes. Therefore, the programmable phase shifter (or inverter) 4 must be capable of realigning the common mode signal to the differential mode signal such that there is a 180° phase

difference between the signals in the frequency bandwidth of the noise suppression filter channel.

As RFI signal frequency increases, the phase difference between the CM and DM will increase beyond 360° (2π rad.) such that phase correction over multiple cycles of the CM signal would be required to realign the CM RFI with the DM RFI noise. Fortunately we can consider RFI as steady state or at least slowly varying over time when the information signal is modulated with a constant carrier. Under such conditions, a phase difference of a few cycles can be tolerated with minimal error. This hypothesis also applies to other types of signal modulation as long as the rate of change of the message signal is much lower than the modulating frequency (carrier). The amplitude of the error signal resulting from the multi-period phase offset is dependent on the difference in propagation delay between the CM and DM with respect to the rate of change of the message signal, or equivalently the frequency bandwidth of the message signal.

Consider a 1 MHz carrier amplitude modulated with a message signal limited to a 6 kHz bandwidth. Assuming that the message signal frequency is represented by fm and the carrier by *fc*. The following equations describe input conditions and the resulting AM signal $s(t)$.

$$s(t) = A_C\left[1 + \mu\left(h_{LPF}(t) * \cos(2\pi f_m t)\right)\right]\cos(2\pi f_c t)$$

$$\text{where} \quad f_m = \begin{cases} 0 & 0 < t < 0.01\,ms \\ 4.0\times 10^{-3} & 0.01 < t < 0.04\,ms \end{cases}$$

$$\text{and} \quad h_{LPF}(t) = \pi f_p \operatorname{sinc}\left(\pi f_p t\right) \quad \text{where } f_p = 6\,\text{kHz}$$

The following graph (Figure 3.9) shows level of noise generated by the difference in signal content due to the large phase offset between the DM and CM signals.

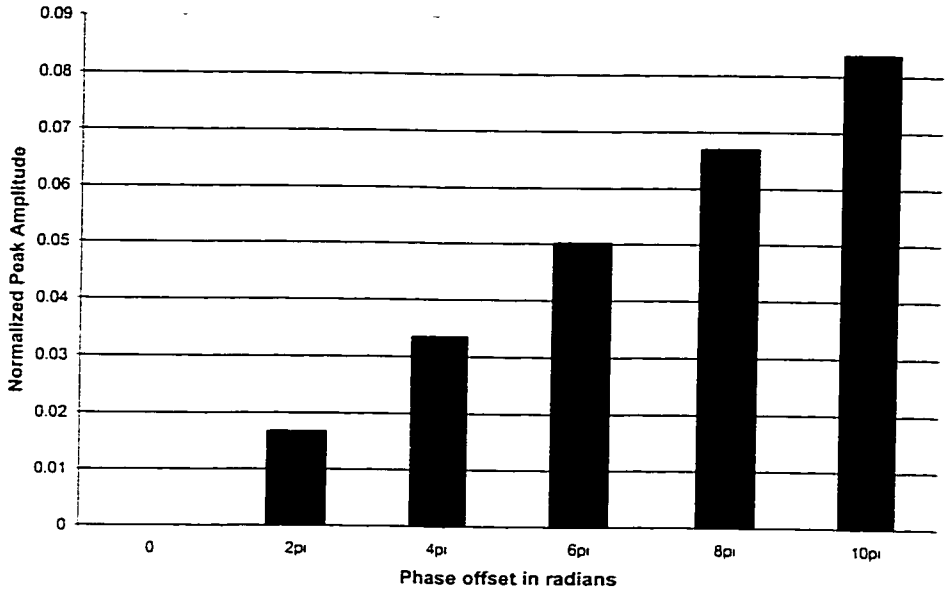

Figure 3.9: Error Due to Phase Mismatch between Identical RF Signals

In addition to the application of phase correction on the CM signal source, gain adjustment is required to attenuate the relatively high level CM RFI signal to levels matching the RFI noise appearing on the DM channel at the input of the receiver. The relationship between the DM and CM signals is not only proportional to the balance of the cable. A factor to account for cable attenuation must be added since, the respective channel attenuation may be different for CM and DM. Gain adjustment is accomplished by gain pad (Adaptive Gain Block) 5 in Figure 3.7.

Once adjusted, the adaptive noise suppression circuitry will cancel a given DM RFI signal source with characteristic matching the phase and gain difference between the DM noise and CM reference signal. Unfortunately since the phase relationship between CM and DM changes over frequency, phase and gain error of other signals on the CM will impact the DM channel. The severity of this impact can range from no significant SNR degradation to a worst case scenario where the reference CM signal is in phase (at the canceling summer) with RFI noise on the DM channel.

Band limiting is required to avoid corrupting the DM channel at sub-optimal frequencies where phase and gain corrections introduced by the ANS circuit

generate additional noise at the output of the canceling summer. The addition of an adjustable band-pass filter 3 (Figure 3.7) at the input of the phase correction filter will prevent the processed cancellation signal from affecting frequencies outside of the RFI disturber bandwidth.

The center frequency of bandpass filter 3 is adjusted to coincide with the center frequencies of the narrow-band noise (RFI) as detected by the adaptive controller 8.

The adaptive controller performs multiple tasks such as spectral analysis of the CM channel to detect and categorize all RFI threats in the operating bandwidth of the host DSL modem. As well the controller regulates the amount of nonlinear phase inversion so that the nonlinear phase delays inherent in hybrid 6, and phase variations between CM and DM channels can be compensated. Finally, the adaptive controller also controls the gain of the adaptive gain block 5. Typically a low speed microcontroller or a low priority real time process can be used to implement the adaptive controller 8, since the real time requirement to perform the above adaptive computations is low.

Spectral analysis of the CM channel can be performed with Fourier analysis on the input signal to locate RFI. Subsequently, each RFI threat can be evaluated for it's noise contribution to the DM signal by performing a cross-correlation of the suspect RFI signal with a band-limited version of the DM signal such that both signals have the same frequency range. The ANS controller would then tune the ANS circuit 3,4,5 to cancel DM noise contributed by the worst RFI disturber. The adaptation algorithm would adjust both the phase and magnitude response of the ANS filters in an attempt to minimize the cross-correlation between the reference CM RFI signal and the DM noise signal. A minimized cross-correlation indicates a suppression of the DM noise signal, and therefore corresponds to an increased SNR. Alternatively, a Quality of Service (QOS) or SNR signal could be used as the feedback signal to the ANS control algorithm.

Many different types of control algorithms can be implemented to control this system, searching for an optimal control technique for ANS is beyond the scope of this thesis. One generalized algorithm is proposed for demonstration purposes.

Figure 3.10, 3.11 and 3.12 compose a flowchart of one possible control algorithm for ANS that could be implemented. This algorithm uses the following variables and data structures:

Mode is the ANS controller State variable. This variable has two possible states. The "adapt" state indicates that the ANS system has detected a RFI noise source that is a threat to the DSL modem. In this state the controller will lock the ANS filter onto the RFI source and execute adaptation algorithms to minimize the cross-correlation between the CM and DM. In the "search" state, the ANS controller monitors the twisted pair for RFI ingress with levels superior to the currently suppressed RFI signal.

RFI_lock is the Data structure containing information on the current RFI signal being suppressed by the system. This structure contains the following variables: "Init_noise_level" which is the initial cross-correlation result when this signal was identified as an impairment to the DSL system. "RFI_frequency" stores the center frequency of the RFI source. "ANS_settings" contains the filter gain and phase settings.

RFI_old is a data structure consisting of a list of the RFI_lock structures. This data structure stores information on previous RFI sources that were cancelled by the ANS system. The generation of a log of past RFI impairments reduces the convergence time of the ANS filter on subsequent appearance of known RFI sources. In essence, the storage of historical data permits the system to learn.

RFI_list is the storage structure for detected CM RFI sources. The list is sorted in descending order such that the highest RFI signal detected on the CM channel is the first element of the list.

Adapt_timer is a counter to force the controller to periodically fine tune the ANS filter. Re-adaptation is necessary since loop conditions and RFI source characteristics may vary over time.

Figure 3.10 is part A of the flow chart diagram for the control algorithm. When the controller is first initialized the variables and data structures are set *1* such that the algorithm will immediately search for RFI threats. Threat analysis is achieved through spectrum analysis *3* of the CM signal and cross-correlation *4* with the DM noise. Following the FFT analysis of the CM channel, the CM spectrum is searched for RF signals. All detected RF signals are sorted with respect to signal strength and stored in the RFI_list structure. The first element of the list, which has the highest signal level, is cross-correlated with the DM spectrum matching the CM RFI center frequency and bandwidth. If the cross-correlation result is lower than the unsuppressed cross-correlation value of the current RFI disturber being suppressed by the system, the first element of the list is deleted. The controller will then proceed to cross-correlate the next element in the RFI_list. Conversely if the result is larger, the data contained in RFI_lock is stored in RFI_old and the data of the fist element of the RFI_list is moved to RFI_lock *6*. The controler will then adapt the ANS filter to cancel the new RFI signal.

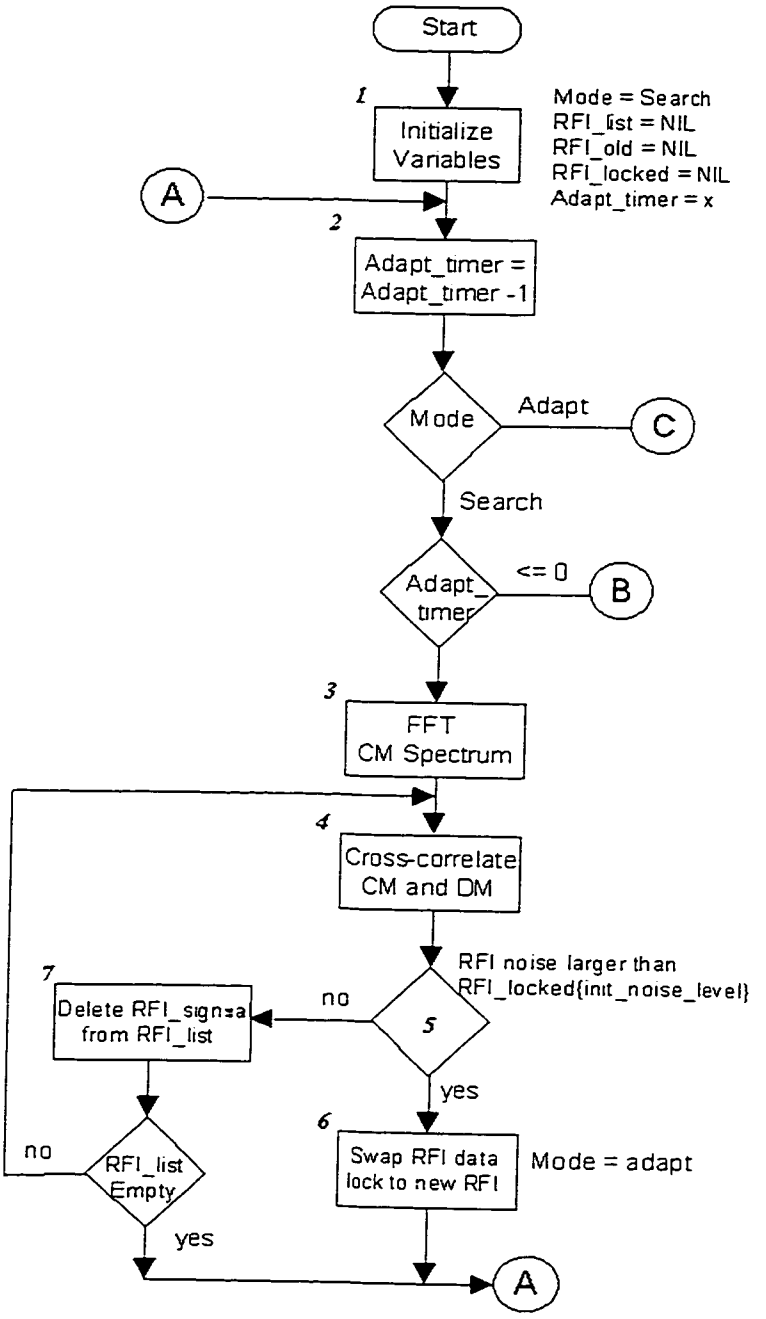

Figure 3.10: ANS Control Algorithm Flow Chart Part A.

In the case where the Adapt_timer has expired, the control algorithm will initiate fine tuning of the ANS filter to insure maximum suppression of the RFI signal in the DM. Figure 3.11 shows the tuning algorithm for the filter. The filter parameters are optimized by comparing the cross-correlation *4* of the CM and DM signals

before and after modification of the filter parameters. A LMS type of minimization algorithm could be used to compute the updated filter parameters *8*. The range of each parameter change must be constrained to prevent degradation in filter performance. On completion of the filter adaptation, the Adapt_timer is reset and the controller state reverts back to Search mode.

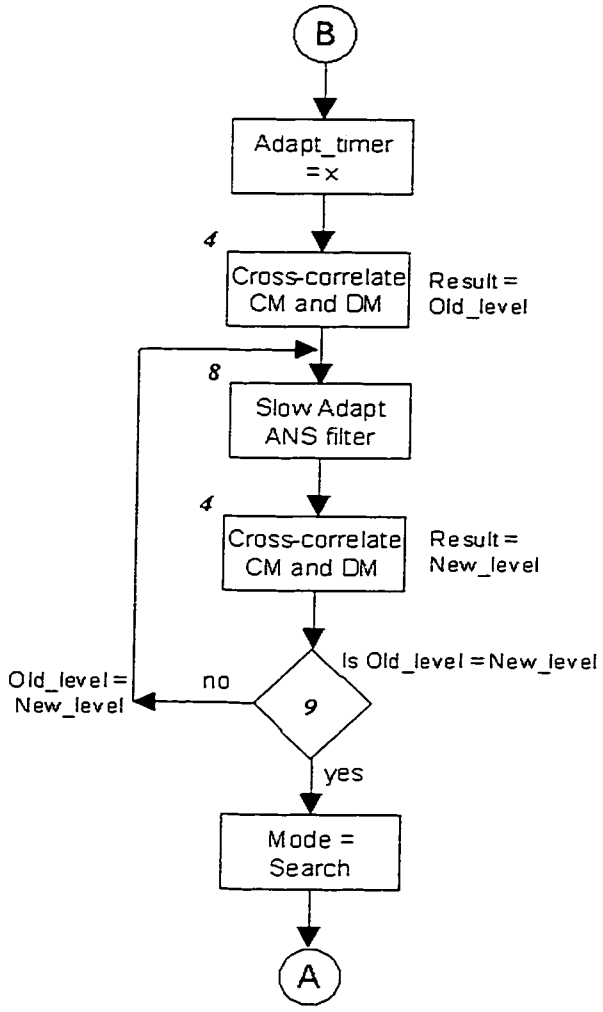

Figure 3.11: ANS Control Algorithm Flow Chart Part B.

Figure 3.12 illustrates the last part of the ANS control algorithm. Whenever the controller detects a new RFI threat in the Search mode, the signal characteristics are compared *10* to previous RFI signal parameters stored in RFI_old. If a match is found, the previous filter data is copied *13* to RFI_lock and the algorithm proceeds to fine-tune the ANS filter to compensate for environmental variations since these

parameters were last used. If the signal characteristics are not found in the RFI_old list, then the controller will rapidly adapt the ANS filter *12* to suppress DM noise generated by the RFI signal. In this condition the error minimization routines used to adapt the filter will have wider parameter constraints than the slow adapt ANS filter *8* routine to minimize convergence time. Once the filter is adapted, the control algorithm changes state to resume searching for other RFI noise sources.

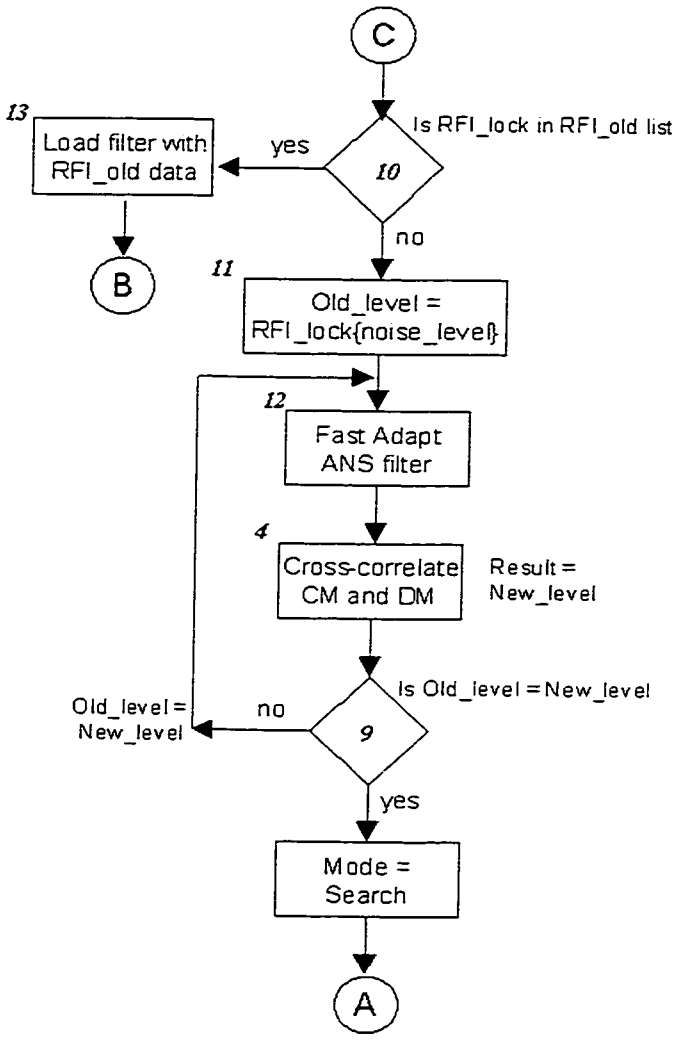

Figure 3.12: ANS Control Algorithm Flow Chart Part C.

Here is a recap of the signal flow through the ANS system starting at the twisted pair input where both the DM and CM signals are presented at line interface 1 (hybrid) as seen in Figure 3.7. The Common mode signal is extracted from the

twisted wire pair by summer 2, filtered by adaptive band-pass filter 3, and then phase inverted by programmable phase inverter 4. The resulting signal is scaled by adaptive gain block 5 and is combined with the differential mode output of line interface 6 to mitigate common mode noise present at the output. The improved differential mode output 7 with higher Signal to Noise Ratio (SNR) is then presented to the receiver.

3.4.2 Multi-channel ANS System

The single channel system presented in Section 3.4.1 can be used as the basis for a multi-channel ANS system. As shown in Figure 3.13, the multi-channel signal suppressor 10 is composed of a group of single channel signal suppressors 11. Additionally, the ANS control algorithm must be upgraded to control n-channels effectively. In other words, additional intelligence is required to properly assign each available ANS channel to selected RFI disturbers such that the overall SNR seen at the receiver is maximized.

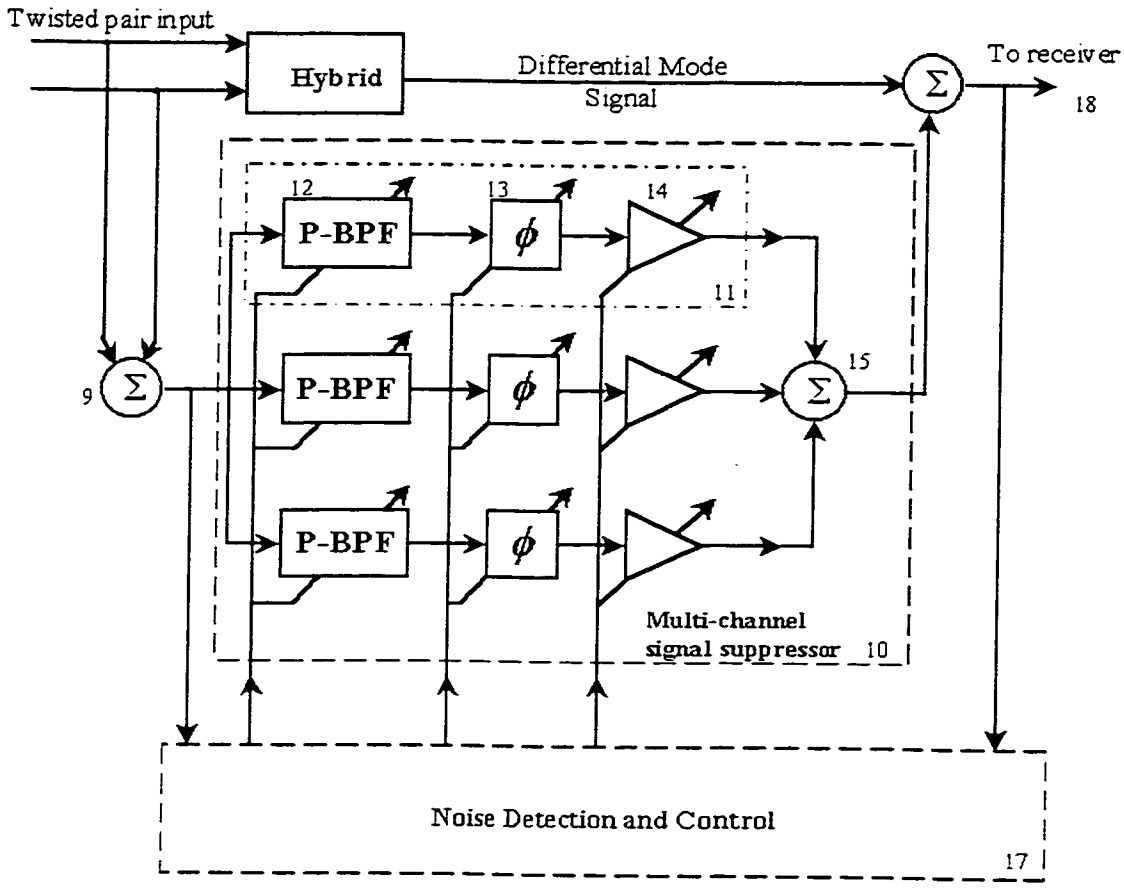

Figure 3.13: Block Diagram of Multi-channel Adaptive Noise Suppressor.

The signal flow through the multi-channel ANS system is as follows: the CM signal extracted by the summer 9, is then processed by the signal suppressor 10. The signal suppressor is composed of a group of processing channels 11, each of which is comprised of a programmable (adaptive) narrow-band bandpass filter 12. The bandwidth and center frequency of the bandpass filter can be programmed to match the bandwidth and center frequency of a narrow-band noise detected by performing spectral analysis of the common mode signal at the adaptive controller. As a result, the output of the bandpass filter will be a narrowband component of the common mode noise. We note that the proposed design can have any number of

processing channels depending on the number of narrowband common mode noise that needs to be suppressed.

Signals from each sub-channel 11 are combined at summer 15. Common mode noise suppression occurs at summer 16 when the phase inverted common mode noise is added to the differential mode signal containing the residual noise.

The noise detection and control unit 17 detects the residual noise at 18 to adaptively modify the parameters of each sub-channel 11 of the multi-channel signal suppressor 10 to minimize the noise at 18. Noise detection is performed by computing the average of the cross-correlation between the differential and common mode signals, as discussed in section 3.4.1.

Spectral analysis of the common mode signal to detect residual noise in differential mode signal can be performed simply by computing Fourier transform of the signal. This approach requires intensive computations and thus a high-speed processor is necessary. Alternatively, to avoid the need of a high-speed processor, spectral analysis is accomplished by sweeping the entire frequency band of the digital subscriber loop incrementally using narrow band bandpass filters 19 and 20, as shown in Figure 3.15. Or alternatively a filter-bank approach could be employed. The sweeping of signal is controlled by a microcontroller 21 and the interactions between the analog components and the microcontroller is provided by the ADC 22 (analog to digital converter) and DAC 23 (digital to analog converter). Radio frequency interference (RFI) could be detected by sweeping the entire frequency band of the common mode signal while differential mode noise could be detected by sweeping the cross-correlation between differential and common mode signals. We note that common mode noise are passband signals and need to be converted into baseband signals to fit into the frequency range of the 22 (ADC) by demodulating the noise with carrier signals. Carrier signals are typically generated by a voltage-controlled oscillator 24 (VCO) whose frequency could be tuned by adjusting input voltage of the VCO.

3.5 *Realization*

Two different implementations of ANS will be presented which seem practical to realize in hardware. The proposed implementations will demonstrate that ANS is a realizable technique. ANS can also be realized through many other implementations, of which the variations will not be discussed here since they are usually driven by the host hardware platform.

3.5.1 Mixed-Signal ANS

The first implementation proposed here is a mixed signal approach using mostly analog components with limited digital processing capability. An alternative configuration where the signal detector and controller are implemented digitally will also be presented.

The Mixed-signal approach consists of the multi-channel signal suppressor block implemented as a fully analog circuit. The implementation of this circuit follows the description in sections 3.4.1 and 3.4.2. The signal detection is also accomplished through analog processing as shown in Figure 3.15. In this architecture, the CM and DM signals are pass-band filtered for subsequent analysis by a pair of programmable analog band-pass filters 19 & 20. The filtered CM and DM output signals from these filters are gain adjusted for optimal signal processing. The CM frequency spectrum is swept to extract information on RFI sources. This is accomplished by varying both the programmable band-pass filter 19 and voltage controlled product modulator 24, shifting the band limited CM test signal to base-band for sampling by the ADC 22, of the micro-controller 21. A spectral map of the common mode channel can be created by measuring the amplitude of the detected signal at each frequency point tuned by the band-pass filter 19 and local oscillator 24. In conjunction with the CM spectral information the controller will need feedback information on the performance of the ANS filter. A cross-correlator is implemented with a low pass filter, sliding average integrator

and multiplier 25. A post ANS processed DM signal, filtered by a programmable band-pass filter 20 with identical parameters as the CM filter 19, is correlated with the band limited CM signal to detect the residual noise present in the DM caused by this CM signal. The controller will then appropriately adjust the ANS filter(s) and Noise detection front end 19, 20, 24, 25 through a DAC 23.

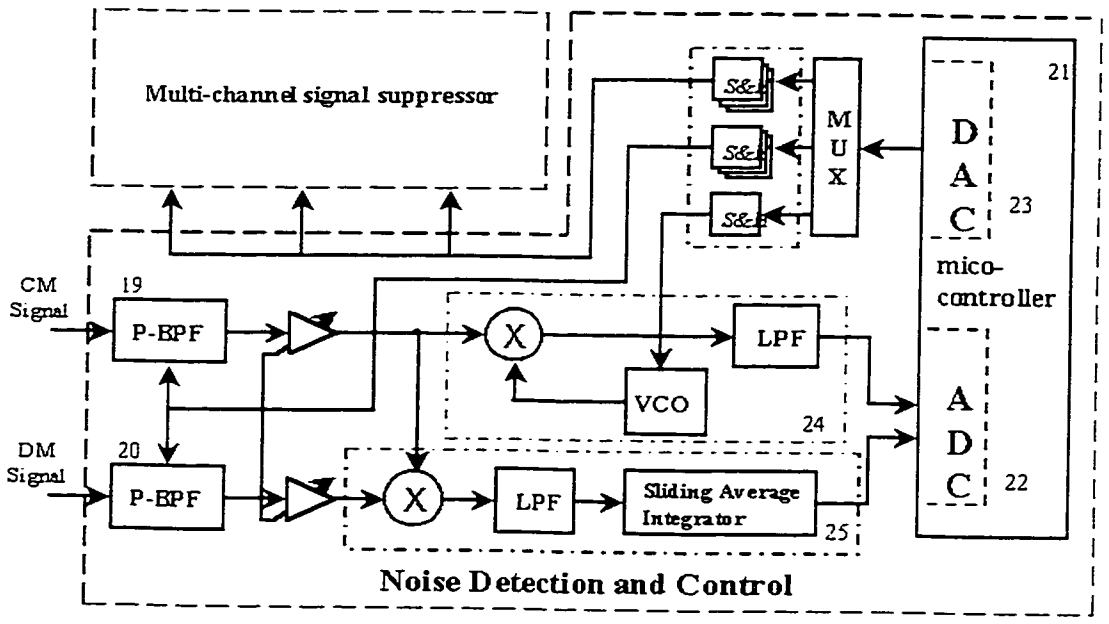

Figure 3.15: Mixed-Signal Noise Detector and Control Sub-system.

Although this is not a cost-effective solution, it does give an idea of the complexities involved in designing an analog implementation of ANS. A more palatable approach would consist of performing the noise detection and control in the digital domain.

By revisiting the Noise detection circuit of Figure 3.15 and adding high speed analog to digital converters close to the variable gain amplifiers in the signal chain, we can eliminate all of the analog hardware involved with noise detection. Figure 3.16 is the modified block diagram of the noise detection and control module.

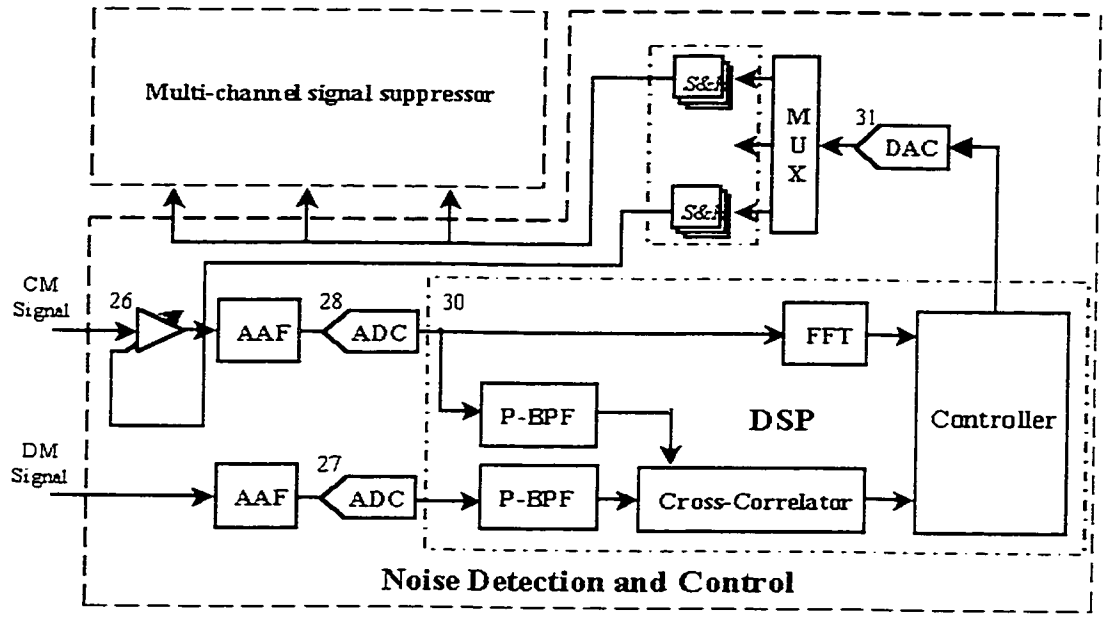

Figure 3.16: Mixed-Signal/DSP Noise Detector and Control Sub-system.

The modified architecture depicted in Figure 3.16, still includes an analog signal suppressor with the addition of a high speed digital signal processor. Converting the noise detection processing into the digital domain requires one additional high-speed ADC 28 for the CM. The DM ADC 27 is in fact the modem ADC. The CM input signal is scaled through an automatic gain control 26 to prevent the ADC from saturating. After gain adjustment, the signal is low-pass filter by an Anti-Alias Filter (AAF) and digitized by the ADC 28. Spectral analysis of the CM channel is accomplished by a fast Fourier transform while residual DM noise is detected by cross-correlation of a pass-band filter version of the DM and CM signals 30. Control of the analog components is achieved through a low speed DAC 31.

There are advantages to a mixed signal implementation: The DM ADC can be protected from saturation conditions by the ANS system under strong RFI ingress levels. The CM ADC is also protected from saturation by the AGC circuit at it's input. As well, depending on the adaptation speed requirements, the noise detection and control can be relegated to a low priority process in a real time operating

environment. The analog ANS filter implementation avoids quantization effects (noise) that must be considered for digital filter designs.

Conversely, the disadvantages for this type of implementation are as follows: The analog circuitry required implementing the ANS filter becomes quite complex if the number of ANS channels is large. As well, complexity also emanates from the need for sub-components of each ANS filter channel to be controllable, since the system is adaptive by definition. Depending on the filter implementation, an analog circuit of this type may be susceptible to stability and noise problems. For a mixed signal design to be cost effective and implementable, the number of ANS channels must be restricted to only a few.

3.5.2 Digital ANS

The Digital implementation of ANS consolidates all system functions into the digital domain, where discrete time signal processing techniques can be used to maximize filtering efficiency.

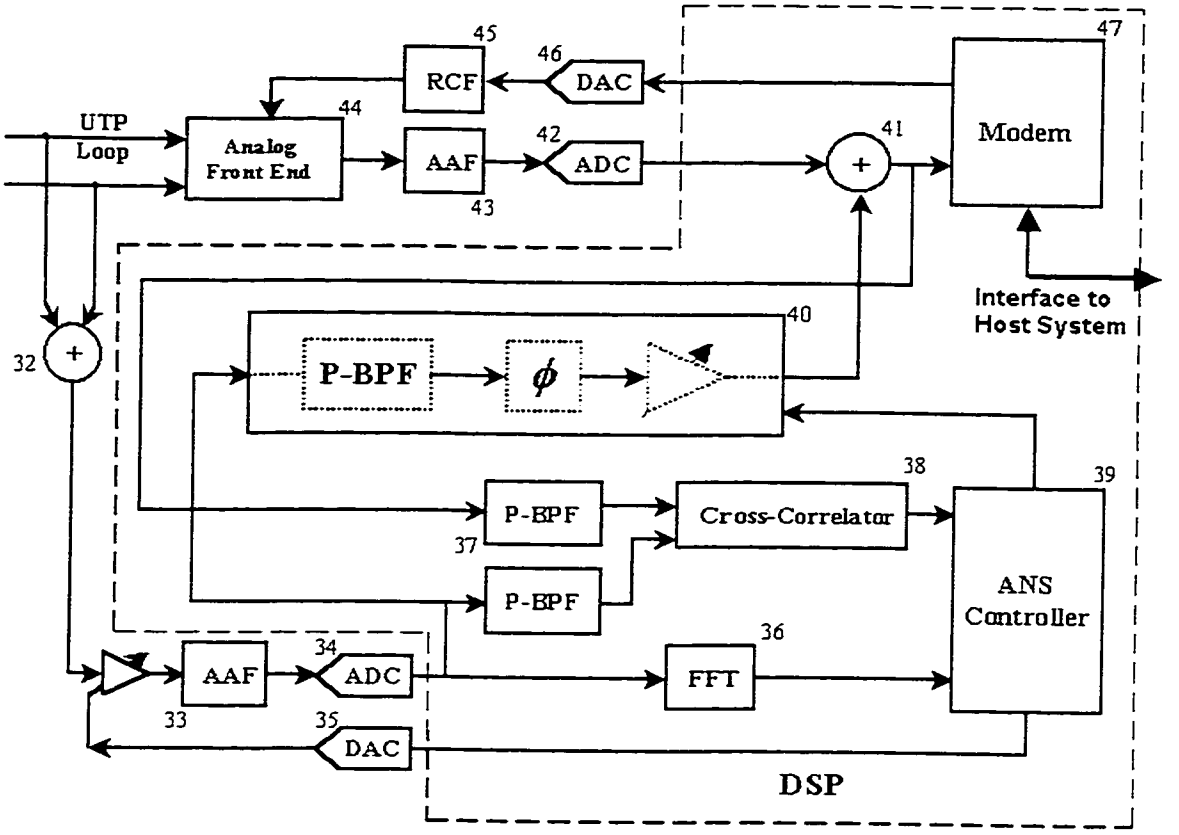

Figure 3.17: Digital/DSP Adaptive Noise Suppressor.

Shown in Figure 3.17 is a functional block diagram of a complete system including the modem, which is represented as one block. It is obvious that the modem is in itself a complex structure, nevertheless for the following functional description only the inter-working of the ANS system with respect to the whole system is of interest.

The digital implementation does require minimal analog signal processing to condition both input signals to properly digitize them. The analog processing, in this case, takes the form of AAF filters for the CM input 33 and DM input 43. In addition an analog summing amplifier 32 is used to extract the CM signal from the twisted pair loop. The CM ADC is protected from input signal overloads by a variable gain stage controlled by a low speed DAC 35. Again the noise detection is accomplished through Fourier analysis 36 and cross-correlation 37, 38 as described

in the mixed-signal DSP implementation. All ANS signal processing is done digitally allowing flexibility of the ANS filter configuration. Theoretically, multiple ANS channels could be processed with a single filter 40, which can perform pass-band, gain and phase corrections at multiple frequencies.

This type of implementation is cost effective to design since it uses much of the same elements as the modem such as DSP engine and ADC. Essentially, ANS can be integrated as an extension to the DSL modem software with minor hardware additions. Prototyping and development can be accomplished rapidly considering that the implementation is software based.

Conversely, one must consider quantization effects and sampling rates for the ADC and in the design of finite precision filters. AS well, the DM ADC could become saturated by strong RFI noise since the input signal can't be attenuated as in the mixed signal ANS case. Additional computing power is needed to realize the complete DSL modem with ANS. With the analog version, ANS processing was achieved independently of the digital portion of the DSL system.

3.5.3 Common Mode Termination Impedance

VDSL documentation, in general, assumes a termination of 50 Ω common mode since this signal is not required at the receiver. However, this termination impedance may cause a significant level of reflections due to the mismatch between the characteristic impedance of the channel and the termination. A noise canceller will therefore need a special front-end circuit to provide correct termination in both modes. An example of CM impedance matching circuit is shown in [15]. Although, CM termination impedance matching is important for effective noise suppression, it is not dealt with here since it is application specific with respect to the modem design.

4 Simulation Model and Results

The ANS concept is verified through simulation of a VDSL system, which includes the RFI cancellation portion of ANS. Not included in this work is the control and adaptation subsystems presented in section 0. Simulation results proving the functional concept of ANS are presented as well as additional data on system sensitivity to parametric changes such as phase and gain errors, and bandpass filter parameter variations.

4.1 Configuration of simulation model

The simulation tests a one-channel noise suppressor in a VDSL environment. The VDSL interference scenario presented in the VDSL system requirements [16], is adapted to a single disturber case for proper evaluation of a one-channel ANS system.

Extension of the simulation to ADSL is not difficult since transmitter and interfere power levels are similar. The potential number of disturbers is significantly lower for ADSL since the operating bandwidth is reduced to only 1 or 2 MHz. Attention must be placed on preserving the external noise floor at −140 dBm/Hz.

4.1.1 Transmitter and Receiver models

A QAM-16 signal is generated from two random streams of 4-PAM symbols to create the message signal (Differential mode). The two PAM signal is raised-cosine filtered with a roll-off coefficient of 0.4 before modulation into respective I and Q-channels of a given carrier frequency. The simulation uses a sampling frequency of 35 MHz, and the carrier frequency as well as the data rate selection is dependent on the loop length used. In this case a loop length of 1 km is used, and therefore the carrier frequency selected is 5 MHz yielding a data rate of 20 Mbps. The

transmitted signal is scaled to fit under the –60 dBm/Hz transmit power mask as defined in [16]. If desired the same signal can be reused in subsequent simulation runs.

Only the Analog Front End (AFE) of the Receiver is modeled. Since this work focuses on signal to noise improvements by processing received signals before treatment by the modem, inclusion of DFE and other modem blocks will not add value to the simulation results. Justifiably, only the preliminary signal processing blocks in the receiver signal chain have been included to emulate the spectral shape of the expected signal at the input of the ANS system.

The Hybrid transformer is modeled with a bridge capacitance set at 10 pF, which gives it about 83 dB balance at 1.1 MHz and 60 dB balance at 17.5 MHz. The 90° phase shift is carried out by multiplying the FFT by sqrt(-1) between $\omega = 0$ and $\omega = \pi$ After performing symmetric extension of the FFT, it is inverted to get a real output.

Front-end analog filtering is included to properly model the susceptibility of a VDSL modem to RFI impairments. The front-end analog filters are designed to band-limit both the CM and DM signals to the frequency region between 1.1 MHz and 8 MHz, which is standard for downstream transmission on 1 km of AWG 26 cable. The reference signal is also passed through the same filter, enabling SIR measurements at the AFE output. The filters are designed with over 60 dB of stopband attenuation with a moderate roll-off between the passband and stopband, a realistic response for analog filters. An 8^{th} order elliptic lowpass filter can achieve 80 dB roll-off at about 1.25 times the cutoff frequency [17].

For convenience these filters are implemented as finite impulse response filters in this simulation. Since FIR filters won't distort signal amplitude and phase as would an equivalent analog filter, the output of the AFE will differ slightly from a real implementation. Although the simulation is limited in this respect, the lower levels of signal distortion are still acceptable since a typical receiver includes adaptive equalization to compensate for channel and filter distortion. With respect to the

ANS system, the same filter distortion applies to both the differential and common-mode signals, therefore it will not affect the operation of the noise canceller.

To complete the VDSL system model Additive White Gaussian Noise (AWGN) is added to the system. Separate sequences of AWGN with PSDs at −140 dBm/Hz are generated and added to the differential and common-mode signals before Signal to Interference Ratio (SIR) calculations.

4.1.2 Interference model

The interference model used in the simulation work is a stripped down version of the RFI threat model presented in the VDSL standards document [19]. For verification and analysis purposes, only one RFI disturber is desired since a one-channel ANS system will be evaluated here. RFI disturbers are injected into the loop at frequencies within the QAM transmission bandwidth with CM power levels ranging from -10 dBm to +30 dBm.

4.1.3 Differential and Common mode transmission models

This simulation uses a two-wire transmission line model to characterize both Differential and Common-mode transmission paths present on twisted pair wire. Using this approach a loop can easily be characterized by RLGC parameterization. Figure 4.1 shows the equivalent T-circuit in terms of RLGC parameters expressed in standard electrical units per unit length.

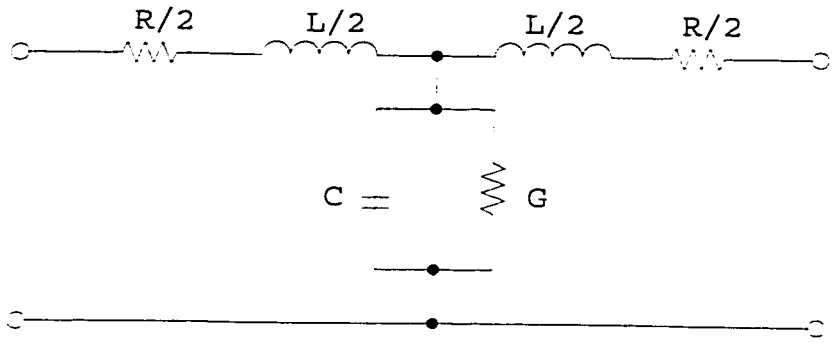

Figure 4.1: Equivalent T-circuit of two-wire transmission line

Given the parametrics of a unit length of twisted pair wire, additional sections of transmission line can be modeled using 2-port networks described later.

As seen in Figure 4.1, the primary constants of the T-network are the series resistance R and inductance L, and shunt capacitance C and conductance G, all expressed in standard electrical units per length.

The series resistance is the parameter that defines the attenuation of the loop. As the frequency of the signal propagating through the cable is increased, the skin effect causes the induced currents to flow closer to the outside surfaces of both wires [13]. This means that the resistance of the loop will rise with frequency. Resistance also varies significantly with temperature, rising by about 4% for each additional 10°C [22]. Above 300 kHz, R is approximately proportional to $\sqrt{f}$ [18]. Below 300 kHz, the resistance increases at a slower rate. Altogether, the resistance for a AWG 26 cable can be modelled by [19]:

$$R(f) = \sqrt[4]{(286.17578)^4 + 0.1476962 \cdot f^2} \quad \Omega/\text{km} \quad (4.1)$$

This equation gives the plot shown in Figure 4.2.

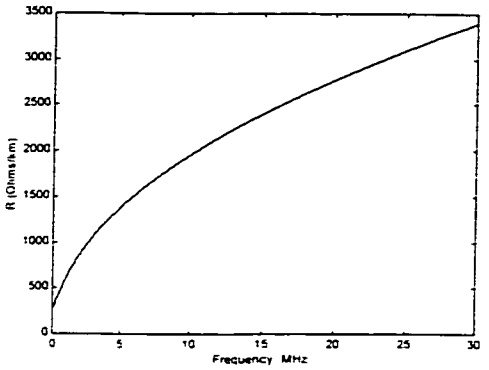

Figure 4.2: Resistance Parameter (R) vs. Frequency.

The L and C parameters define the speed at which the signal propagates through the cable. Again, the skin effect causes the inductance L to decrease with rising frequency, as modelled by [19]:

$$L(f) = \frac{675.36888 + 488.95186 \cdot \left(f / 806.33863\ \text{Hz} \right)^{0.92930728}}{1 + \left(f / 806.33863\ \text{Hz} \right)^{0.92930728}} \quad \mu\text{H/km} \quad (4.2)$$

This equation gives the plot shown in Figure 4.3

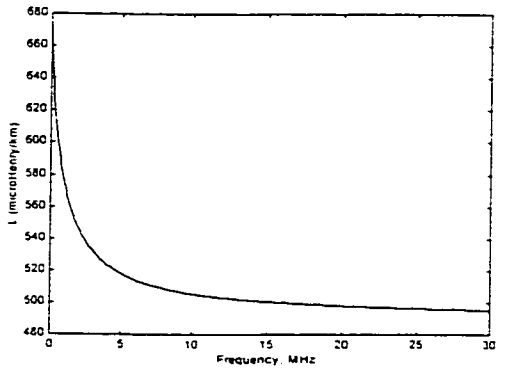

Figure 4.3: Inductance Parameter (L) vs. Frequency

Alternatively the capacitance C of the loop, depends on the distance between the wire, twist length, as well as the dielectric medium used as the insulating material

[13]. The capacitance is approximately 49 nF/km at all frequencies for 26-gauge cable.

Finally, the conductance G is also contributes to the attenuation effects, but is usually negligible compared to the much larger series resistance R. G depends primarily on the dielectric medium, and can be modeled as [19]:

$$G(f) = 43 \cdot f^{0.7} \quad \text{nS/km} \quad (4.3)$$

This equation gives the plot shown in Figure 4.4

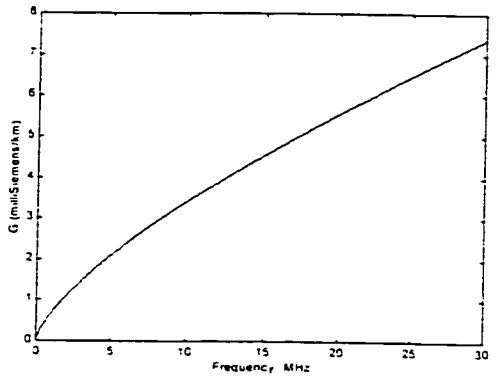

Figure 4.4: Conductance Parameter (G) vs. Frequency

The propagation constant ρ and the characteristic impedance Z_0 can be defined with the RLGC transmission line parameters. These are developed in [9] by applying the Kirchoff voltage and current laws to an incremental section of the loop. The propagation constant is given by:

$$\rho = \alpha + j\beta = \sqrt{(R + j\omega L) \cdot (G + j\omega C)} \quad (4.4)$$

where ω is the radian frequency. The real part of the propagation constant, α, is the attenuation constant, and is expressed in Nepers per unit length (1 Neper = 8.686 dB). The attenuation constant for AWG 26 cable is plotted, in dB/km, as shown in Figure 4.5. The imaginary part of ρ, β, is phase constant, and is expressed in

radians per unit length. The other secondary constant is the characteristic impedance Z_0 expressed in Ohms, and is independent of cable length:

$$Z_0 = \sqrt{\frac{(R + j\omega L)}{(G + j\omega C)}} \quad (4.5)$$

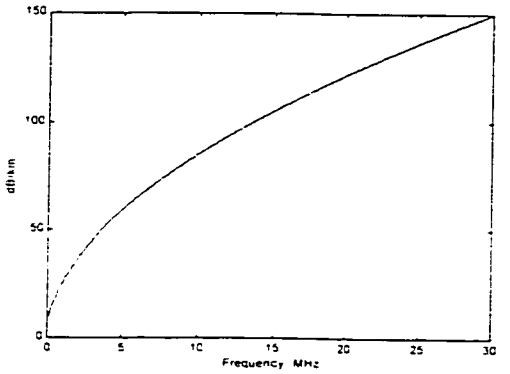

Figure 4.5: Attenuation Constant (α) vs. frequency.

By examining the following equation describing signal propagation in a lossy transmission line [20], one can see the relationship of these parameters on a signal propagating through a twisted pair loop:

$$I(d) = I_0 \cdot e^{-\rho d} = I_0 \cdot e^{-\alpha d} \cdot e^{-j\beta d} \quad (4.6)$$

Here, $I(d)$ is a phasor quantity describing the differential current in the loop, and d is the distance from the transmitter. I_o is the current at the transmitter end of the loop, and can be estimated from the input power P_{in} using:

$$I_0 = \sqrt{\frac{2 \cdot P_{in}}{Z_0}} \quad (4.7)$$

It is assumed for equation (4.7), that I_o current is a peak-peak value and that the input signal is not applied through any device, which causes an insertion loss. The model described by (4.6) and (4.7) will be expanded into a full two-port matrix representation.

All loop sub-components such as sections with different gauge wire and bridged taps, can be represented as a chain of two-port equivalent circuits as shown in Figure 4.1. Mathematically manipulating the propagation constant of a wire section with length d into an ABCD two-port representation allows us to multiply all of the corresponding two-port matrices together, to create a single matrix modeling the entire loop. Consequently, the transfer function of the loop can be computed from this matrix.

A development of two-port modeling for twisted-pair wire is given in [19], and will not be entirely reproduced here. In general, the loop is represented as:

$$\begin{bmatrix} V_1 \\ I_1 \end{bmatrix} = \begin{bmatrix} A & B \\ C & D \end{bmatrix} \cdot \begin{bmatrix} V_L \\ I_L \end{bmatrix} \quad (4.8)$$

where V_1 and I_1 are the voltage and current on the loop at the transmitter end, and V_L and I_L are the voltage and current at the load placed on the secondary side of the receiver's hybrid device. The two-port matrix for a homogeneous section of loop with length d (in km) may be expressed by equation (4.9) at any frequency, where ρ is the propagation constant [19].

$$\begin{bmatrix} A & B \\ C & D \end{bmatrix} = \begin{bmatrix} \cosh(\rho d) & Z_0 \cdot \sinh(\rho d) \\ \frac{1}{Z_0} \cdot \sinh(\rho d) & \cosh(\rho d) \end{bmatrix} \quad (4.9)$$

Using (4.8) and $Z_L = V_L / I_L$, the following transfer function can be found:

$$H(f) = \frac{V_L}{V_1} = \frac{Z_L}{A \cdot Z_L + B} \quad (4.10)$$

The magnitude of $H(f)$ is called the insertion loss. Note that this transfer function does not relate the voltage at the load to the voltage at the transmitter, but to the voltage at the transmit end of the loop.

Given a 1-km 26-gauge cable terminated in 100 Ω, $H(f)$ will have the transfer function shown in Figure 4.6. Appending the conjugate of $H(f)$ to itself

symmetrically and taking an inverse Fourier transform will yield the impulse response for the loop. Figure 4.7 shows the impulse response of the transfer function *H(f)* of Figure 4.6, when a sampling frequency of 35 MHz is used. This plot clearly shows the propagation delay and phase distortion caused by the loop. In this case we see a propagation delay of aproximately180 samples (or 5 microseconds), as well since the impulse response is not a single spike, some phase distortion of the transmitted signal will occur. This dispersion is caused primarily by the slight dependence of L on frequency, and is the reason why inter-symbol interference (ISI) occurs [19].

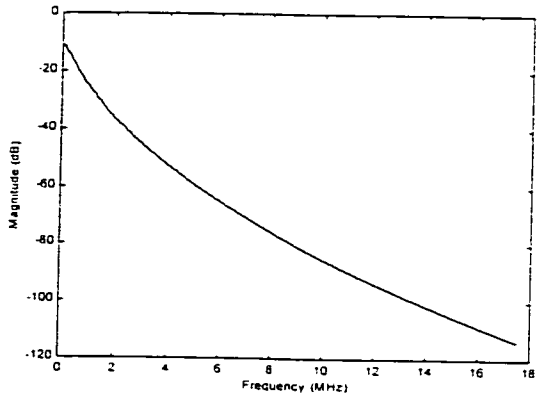

Figure 4.6: Insertion Loss vs. Frequency (1 km of AWG 26 wire)

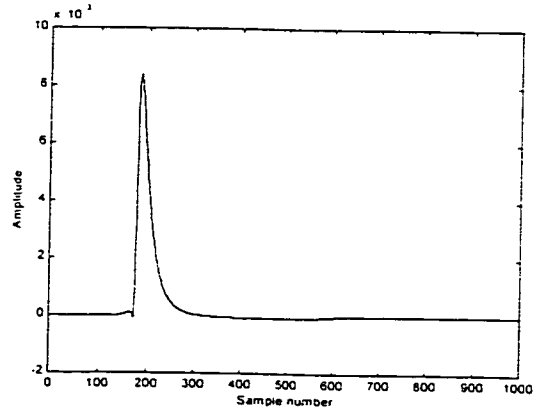

Figure 4.7: Impulse Response of Differential mode (1 km AWG 26, f_s = 35 MHz).

For simulation purposes, the common mode current path exists from the twisted pair wires through the cable shield. Where the loops pair is considered as one wire of the two-wire transmission line, and the cable shield as the other. The decision to use this type of model is driven by the following issues: Very little information has been published on common-mode characteristics of twisted pair wire. As well, the common mode characteristic impedance of unshielded cable is highly dependent on its environment, and will vary significantly from one loop to the next as discussed in section 2. A shielded cable provides a repeatable, controlled environment where simulation can be easily correlated with laboratory experimentation.

Since the common-mode signal sees the two wires of the cable as a single conductor, it is expected that the twisted-pair loop will have half the resistance as it has in the differential case [13]. As well, the return path through the cable shield is assumed to have much less resistance than the loop. Thus, it is reasonable to estimate that the total common-mode resistance R_{cm} will be 0.5 to 0.55 times the differential resistance R_{dm}. Also, the common-mode capacitance per unit length is slightly less for the common mode configuration, than it is for differential. The characteristic impedances of the two modes for a shielded twisted pair cable at 1 MHz are $Z_{0cm} \cong 215\ \Omega$ and $Z_{0dm} \cong 100\ \Omega$. Since $Z_{0cm} = \sqrt{L_{cm}/C_{cm}}$ at high frequencies, if C_{cm} is estimated to be $0.95 \cdot C_{dm}$, then it is reasonable to expect $L_{cm} = 4.4 \cdot L_{dm}$. [13] Neglects the conductance for both modes, but it is likely to be marginally higher in common mode because the shield is further away from the pair than the twisted pair wires are from each other.

Once again from [13], it is known that the cable's attenuation coefficient is about 4.4 dB/km at 1 MHz, without accounting for termination. As discussed in section 3.5.3 and according to the model developed above, the limiting value of the characteristic impedance of the CM channel (Z_{0cm}) is approximately 210 Ω at very high frequencies. Using this termination model gives the common-mode insertion loss in Figure 4.8, and the impulse response of Figure 4.9.

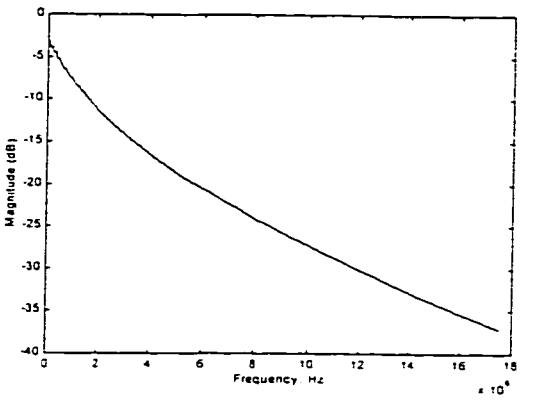

Figure 4.8: Common mode Insertion Loss of 1 km AWG 26 cable

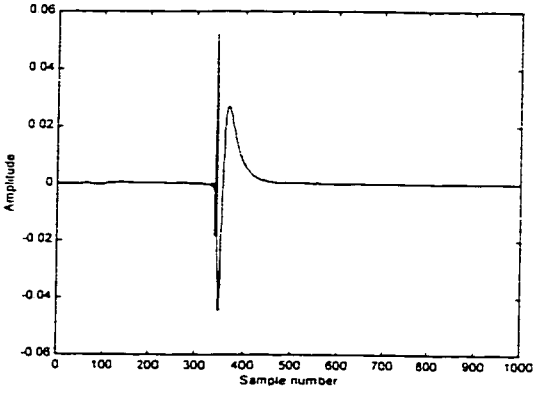

Figure 4.9: CM Impulse Response of 1 km AWG 26 cable (f_s = 35 MHz)

4.1.4 Loop Imbalance Model

As previously defined in section 2.1.3 by equation 2.1, longitudinal balance is the ratio between the common-mode voltage V_{cm} of the cable with respect to ground, and the differential voltage V_{dm} between the two wires of the cable [21]. To meet specifications for telephone use, longitudinal balance must be at least 60 dB at 1,004 Hz, but requirements on levels for other frequencies have not been set [22]. As a result, it is difficult to find a general model for cable balance [17]. From statistical data of loop plant measurements, loops are likely to have a balance of between 50 to 60 dB at frequencies below 100 kHz. Above 100 kHz, barring

defects in the loop plant, longitudinal balance degrades at about 12 dB decade, and may drop as low as 20-30 dB at VDSL frequencies [13, 21, 23]. A worst case assumption would be a loop with only 30 dB balance at low frequencies, and as little as 10 or 15 dB at the upper frequency range of the VDSL spectrum [17, 24]. The balance of a typical twisted-pair cable is shown in Figure 4.10.

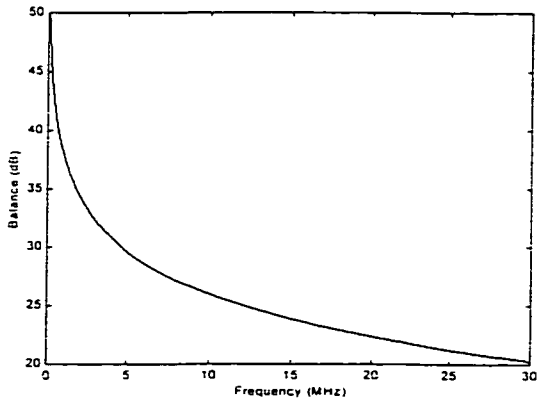

Figure 4.10: Typical Twisted Pair Cable Balance

At high frequencies, the DM characteristic impedance given by equation below is dominated by the reactive elements of the two-wire transmission line model, and can be approximated as:

$$Z_{0dm} = \sqrt{\frac{L}{C}} \quad (4.11)$$

Using equation (4.2) or by extrapolating an approximate value of L from Figure 4.3, it can be verified that at 1 MHz $Z_{0dm} \cong 100\ \Omega$. At higher frequencies, Z_{0dm} only drops slightly from this value [22].

In contrast to a DM signal, a CM signal propagating through a shielded cable sees the twisted pair as a single conductor, in this case the current return path for this mode is through the cable shield. The shield can be considered as a thick conductor with much less resistance than the 26-gauge wire comprising the UTTP loop. Therefore, it is expected that the CM resistance per unit length will be less than its

differential counterpart. Considering that the relative distance between the shield and the loop pair is greater than the distance between the pair wires, the inductive coupling between the pair and the shield is substantially smaller than the coupling between the two wires of the pair. Thus, the CM inductance per unit length of each wire is higher than for the DM. Finally, the CM capacitance per unit length is only slightly less than the DM capacitance, and the conductance is usually negligible [13].

The increased inductance L and unchanged capacitance C, indicates that the CM characteristic impedance Z_{0cm} of a single wire should be larger than Z_{0dm}. [13], gives 430 Ω as a good approximation for AWG 26 cable at 1 MHz. Since both wires of the loop pair are in parallel, the overall CM impedance Z_{0cm} is approximately 215 Ω. Since, EM waves travel down a transmission line by continually exchanging energy between the electrical and magnetic elements, as modeled by the capacitor and inductor lumped-elements in the transmission line model, the CM presents a greater impedance to this energy transfer (i.e.; $Z_{0cm} > Z_{0dm}$) [25].

As a consequence, the speeds at which the two waves travel along the transmission line are not identical. At high frequencies, the envelope delay of the wave can be approximated by $\sqrt{L \cdot C}$ [18], and the group velocity is simply the inverse of the envelope delay [25] as illustrated by equation 4.12.

$$v = \frac{1}{\sqrt{L \cdot C}} = \frac{1}{C \cdot Z_0} \quad (4.12)$$

Since the transmission line capacitance C is approximately equal for both the CM and DM, it is clear that the CM wave will travel at approximately half the speed of the DM wave. At high frequencies, the speed of the differential wave can be found by equation 4.13:

$$v_{dm} = \frac{1}{(49\times10^{-9}\ \text{F/km})\cdot(1\ \text{km}/1000\ \text{m})\cdot(100\ \Omega)} = 2.04\times10^{8}\ \text{m/s} = 0.68c \quad (4.13)$$

where c is the speed of light.

Assuming an identical capacitance value for the CM, the propagation speed of this mode is $v_{cm} = 0.32c$. Accounting for inaccuracies due to high-frequency approximations, these results are consistent with the measured values given in [13] for an AWG 26 cable at 1 MHz, where v_{dm} and v_{cm} were found to be about $0.65c$ and $0.34c$ respectively.

4.1.5 Attenuation and phase distortion

Cable attenuation and phase distortion is carried out using the impulse responses generated by the equations generated above. In cases where the RFI is injected on the loop away from the receiver, the channel is modeled with two impulse responses each modeling a section of loop. When cascaded together these responses will model the full loop length. The impulse response modeling the first section of loop from the transmitter to the RFI injection point is computed using the characteristic impedance Z_{0dm} and Z_{0cm} as the respective CM and DM loads. By convolving both impulse responses together, this result in a response that closely matches the impulse response generated for a full loop length case.

RFI noise sources are coupled to the loop CM channel directly while the DM coupling is scaled with a user-specified balance as a constant value from DC to 1.6 MHz. Additional scaling beyond 1.6 MHz is applied to produce a 12 dB/decade declining slope in the upper VDSL frequency range.

Special attention is required to properly simulate the cable imbalance to ensure conservation of energy between the RFI signal source energy and the energy distributed to both modes of the loop. As discussed in section 2.1 Cable imbalance

is caused by differing impedance to ground for each wire of the loop pair. In other words, one signal is either attenuated and/or phase-shifted differently than the other. One can work out a general solution to relate attenuation and phase shift to balance, but it is easier to assume that the phase shift is zero. With respect to the ANS system, the presence of an additional phase shift at the RFI injection point has negligible effect since the system must compensate for phase shifts caused by differing CM and DM propagation delays. Not accounting for phase, two signals propagating down the loop on each wire with respect to ground can be described by equation (4.14).

$$\begin{aligned} s_1(t) &= \cos(\omega t), \text{ and} \\ s_2(t) &= A\cos(\omega t) \end{aligned} \qquad (4.14)$$

A is a scaling factor describing the amplitude of signal s_2 relative to signal s_1, and is assumed to be between 0 and 1. The CM signal at the end of the loop is $s_1(t)+s_2(t)$, and the DM signal is of course $s_1(t)-s_2(t)$. Referring to equation (2.2), the balance can be expressed as equation (4.15) in this situation.

$$B = 20 \cdot \log_{10}\left(\frac{1+A}{1-A}\right) \quad \text{dB} \qquad (4.15)$$

Figure 4.11 shows a graph of A as a function of balance generated from equation (4.15).

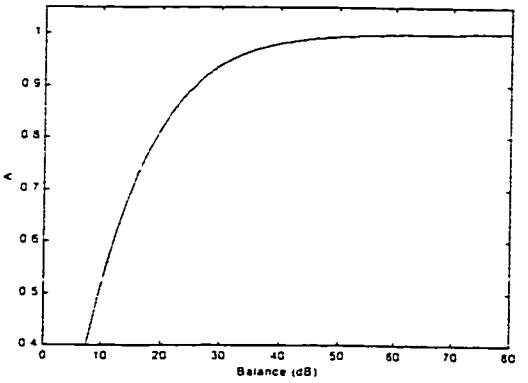

Figure 4.11: Scaling Factor *A* vs. cable balance

The vector of A versus frequency for a desired cable balance, as interpolated from Figure 4.11, can be used to design a linear-phase filter. This filter is used to scale a second copy of the CM signal, which is used in conjunction with the original signal to generate the component that leaks to DM and the component that remains in CM by respectively subtracting or adding the two signals. The same approach is used with the differential signal, so that the total power on the two wires remains constant. If the filter has a sufficient number of coefficients, this method achieves balances very close to the desired characteristics.

4.1.6 Signal to Interference (RFI) Ratio.

The SIR requires an unadulterated reference signal to compute the level of noise present in a given channel, therefore in parallel with the CM and DM signals a reference signal is also generated. This signal is an attenuated but otherwise uncorrupted version of the information signal propagated on the DM and it is used as the correct value of the signal, when average signal power calculations are performed. Since the DM and CM signals at the receiver have zero mean in this simulation model, SIR can be expressed as the ratio of the variance of the signal and noise as shown in equation 4.16.

$$SIR_{(dB)} = \frac{10 \cdot \log_{10}\left(\sigma^2(signal)\right)}{10 \cdot \log_{10}\left(\sigma^2(noise)\right)} \quad (4.16)$$

4.1.7 ANS Models

Bandpass filtering of the CM signal is accomplished with an IIR filter to minimize signal delay within the pass-band. This filter implements a Butterworth filter of variable order, pass-band width and transition band slopes. In all cases the stop-band has a signal rejection level of not less than 40 dB. Table 2 lists the parameters of each bandpass filter used in the ANS simulation.

Table 2: Bandpass filters

Filter	Center Frequency	Pass-band Bandwidth$_{3dB}$	Filter Roll-off	-50dB attenuation frequency
1	1.280 MHz	538.1 kHz	500 dB/decade[3] 684 dB/decade	793.4 kHz 1.934 MHz
2	1.280 MHz	185.1 kHz	575 dB/decade[3] 724 dB/decade	1.186 MHz 1.372 MHz
3	1.280 MHz	200.7 kHz	450 dB/decade[3] 574 dB/decade	906.3 kHz 1.792 MHz
4	1.280 MHz	571.4 kHz	400 dB/decade[3] 546 dB/decade	703 kHz 2.046 MHz

Phase compensation between the CM and DM signals is achieved with two allpass filters, one filter performs the coarse phase compensation on the DM channel while the other accomplishes fine phase compensation on the CM channel. The bulk of the phase correction is applied to DM since it is desirable to preserve a linear phase relationship for this mode. Conversely the cancellation signal generated from the CM is narrowband filtered and as such only requires phase correction within the passband. Additionally, linear phase allpass filters can only modify phase by a multiple of pole-zero pairs, limiting the number of delay values this type of filter can generate. Alternatively, allpass filters with non zero poles can generate an infinite number of delay values for any given frequency by sacrificing phase linearity. Therefore, the remaining phase adjustments required to align the cancellation signal to the DM signal is accomplished with the bandpass filtered CM signal.

[3] The High pass IIR filters used to create the bandpass filters exhibited a digital noise floor significantly higher than would be assumed from these numbers. The noise floor for each filter is as follows: filter 1 = -131dB, filter 2 = -154dB, filter 3 = -287dB, and filter 4 = -286dB.

Gain compensation is applied to the CM signal after bandpass filtering and phase adjustment.

4.2 Test Conditions and Results

4.2.1 SIR Reduction Performance of ANS system with respect to RFI Power Levels and Loop Balance

The first test case presented in this series of simulations demonstrates a reduction of SIR through the introduction of the ANS circuit. The test configuration consists of a QAM signal transmitted over a 1-km loop with one RFI disturber centered at 1.28 MHz and injected at two different distances, 175 m and 500 m. As well, measurements with respect to RFI power level and loop balance are presented to demonstrate the performance of this system under expected operating conditions. Results of ANS performance with respect to RFI power levels are presented in Table 3, for an RF signal injected 175m from the receiver on cable balanced to 40dB at low frequency. Table 4 shows the effect of cable balance on ANS noise suppression performance given that the RFI power level is fixed at 10 dBm. Figure 4.12 show the PSD of the DM signal (QAM) and the CM RFI noise source. As expected, due to limited cable balance, part of the RFI (spike) appears in the QAM signal spectrum. Figure 4.13 shows the PSD of both the DM signal and the CM noise source. With ANS activated, the RFI noise spike seen in the previous figure has been removed form the DM signal spectrum.

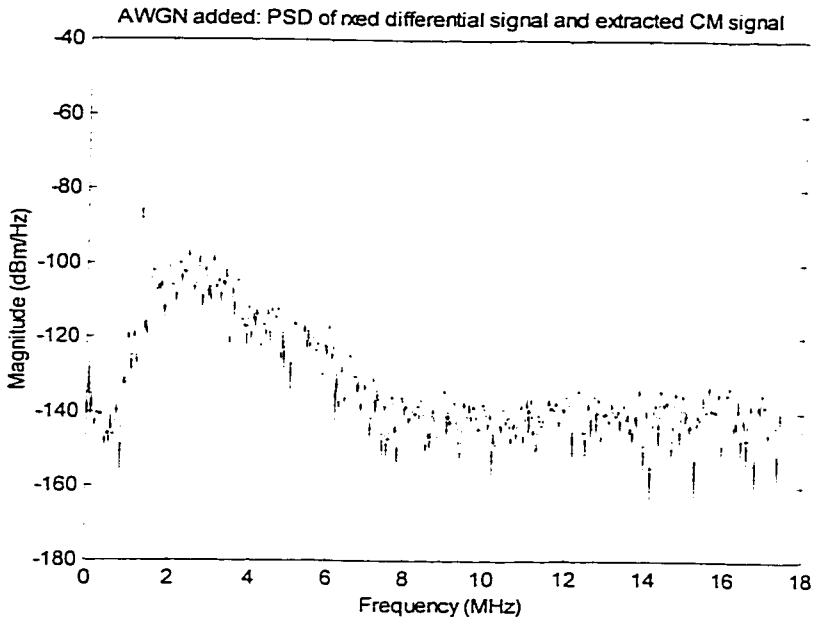

Figure 4.12: Power Spectral Density of DM signal and CM noise with ANS deactivated.

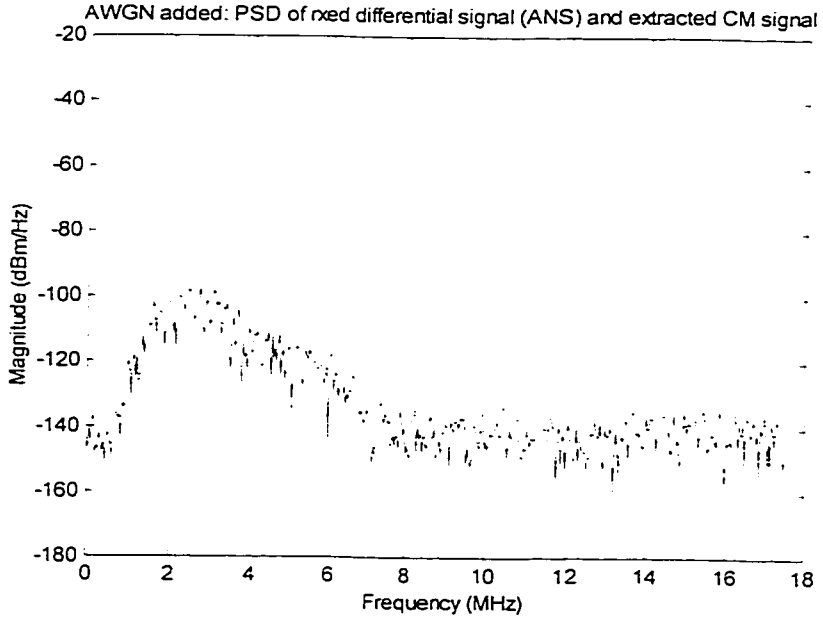

Figure 4.13: Power Spectral Density of DM signal and CM noise with ANS active.

Table 3: 1 km loop with 40dB loop balance, RFI injected at 175m from receiver.

RFI Level	SIR (no ANS)	SIR (with ANS)	RFI reduction
30 dBm	-4.2492 dB	34.4944 dB	38.7436 dB
20 dBm	5.3441 dB	34.5696 dB	29.2255 dB
10 dBm	17.2937 dB	34.6465 dB	17.3528 dB
0 dBm	26.8996 dB	34.139 dB	7.2394 dB
-10 dBm	32.2341 dB	34.2054 dB	1.9713 dB

Table 4: 1 km loop with RFI power level at 10dBm, RFI injected at 175m from receiver.

Loop Balance	SIR (no ANS)	SIR (with ANS)	RFI reduction
60 dB	17.9217 dB	41.8032 dB	23.8815 dB
40 dB	17.2937 dB	34.6465 dB	17.3528 dB
30 dB	15.2179 dB	25.2787 dB	10.0608 dB
20 dB	14.2446 dB	16.4135 dB	2.1689 dB

Results of ANS performance with respect to RFI power levels are presented in Table 5, for an RF signal injected 500m from the receiver on cable balanced to 40dB at low frequency. Table 6 shows the effect of cable balance on ANS noise suppression performance given that the RFI power level is fixed at 10 dBm.

Table 5: 1 km loop with 40dB loop balance, RFI injected at 500m from receiver.

RFI Level	SIR (no ANS)	SIR (with ANS)	RFI reduction
30 dBm	4.9196 dB	35.1406 dB	30.221 dB
20 dBm	17.2582 dB	35.2613 dB	18.0031 dB
10 dBm	24.888 dB	35.3325 dB	10.4445 dB
0 dBm	31.4999 dB	35.2587 dB	3.7588 dB
-10 dBm	34.939 dB	35.2497 dB	0.3107 dB

Table 6: 1 km loop with RFI power level at 10dBm, RFI injected at 500m from receiver.

Loop Balance	SIR (no ANS)	SIR (with ANS)	RFI reduction
60 dB	26.0823 dB	54.3885 dB	28.3062 dB
40 dB	24.888 dB	35.3325 dB	10.4445 dB
30 dB	23.1882 dB	25.3439 dB	2.1557 dB
20 dB	16.2518 dB	16.6035 dB	0.3517 dB

Bandpass filter 1 was used in all simulation cases presented in Table 3 to Table 6.

Results show that the RFI suppression performance of the ANS system is such that the SIR at the receiver increases to between 34 and 35 dB with ANS active irrespective of the initial SIR of the channel. These results assume a loop balance of 40dB at low frequency.

ANS performed equally well with injection points at 175m and 500m from the receiver. Nevertheless, total RFI noise reduction gain for 500m is less than 175m due in part to the maximum signal attenuation of the ANS circuit and signal attenuation from the twisted pair loop. The maximum SIR limit provided by the ANS signal processing chain, is a byproduct of accumulated processing errors such as gain, phase and filter frequency response mismatches.

Considering typical telephone access plant conditions, experimentation with RFI injection distances beyond 500m is of minimal interest since DM noise from CM RFI sources are naturally attenuated by the twisted pair cable. As well an RFI source with equivalent signal power if coupled farther from the receiver, implying that the RFI injection point is closer to the transmitter, will have less of an impact on the DM signal. The DM signal is proportionally stronger to the RFI disturber closer to the transmitter since it has not been attenuated by the cable loss, as would be seen closer to the transmitter. Finally, at the loop pair approaches the CO, immunity to CM noise increases as a consequence of additional shielding provided by the construction of feeder cable and the tremendous number of loop pairs contained within the cable. Therefore, the dominant impairment in this section of the loop plant is crosstalk from adjacent cable pairs not RFI.

Conversely and as expected, ANS performance is dependent on loop balance. Depending on the available loop balance, gains in SIR range from 0.3 dB for 20 dB loop balance to 23 dB at 60 dB loop balance given an RFI source power level of 10 dBm. Typically 30 dB loop balance is the worst case balance for usable loop plant for voice (POTS). Under such conditions ANS still provides a respectable SIR gain of 10 dB[4].

4.2.2 Sensitivity to Gain Error.

The second test case evaluates the sensitivity of the ANS system to gain error in the ANS filter loop. A 1 km loop having 40 dB balance, as described in section 4.2.1, was used as the loop configuration for this experiment. As well the CM RFI was injected at 175m from the receiver with two different power levels (10 and 30 dBm). SIR results for both 10 dBm and 30 dBm RFI injection levels are presented in Table 7 and graphed in Figure 4.14.

[4] RFI level of 10 dBm is assumed and injected at 175m from the receiver.

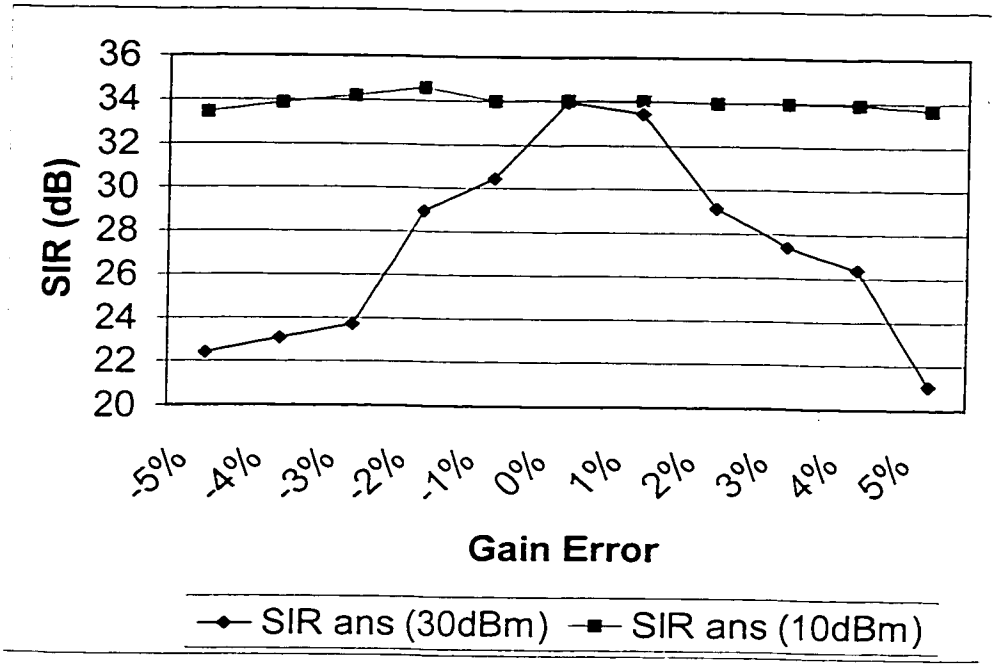

Figure 4.14: Effect of gain error on RFI suppression.

Table 7: Impact of ANS Filter Gain Error on SIR levels.

ANS Gain Error	SIR (30dBm RFI)	SIR (10 dBm RFI)
-5%	22.4004 dB	33.4507 dB
-4%	23.0616 dB	33.8778 dB
-3%	23.723 dB	34.1784 dB
-2%	28.9637 dB	34.5976 dB
-1%	30.4624 dB	33.9951 dB
0%	33.9612 dB	34.0448 dB
1%	33.4366 dB	34.0337 dB
2%	29.1477 dB	33.9404 dB
3%	27.4216 dB	33.9387 dB
4%	26.3717 dB	33.9182 dB
5%	21.0655 dB	33.671 dB

Bandpass filter 1 was used in all simulation cases presented in Table 7.

The data collected from the sensitivity to gain error experiment indicates that gain error has little effect on SIR for low RFI injection levels. For low levels, limitations in the ANS circuitry dominate the SIR figure. Conversely, high RFI levels tend to dominate the SIR figure, and therefore gain matching becomes critical. From the presented data, a gain error of ± 2% is tolerable for an impact of 4 to 5 dB on the SIR performance at 30 dBm RFI power levels. 30 dBm is the worst case RFI power level expected [16]. Current Automatic Gain Control (AGC) circuits can provide precise gain control such that this gain error could be virtually zero.

4.2.3 Sensitivity to Phase Error

The fourth test case group assesses the sensitivity of the ANS system to phase error between the DM and canceling signals. SIR results for both 10 dBm and 30 dBm RFI injection levels are presented in Table 8 and graphed in Figure 4.15.

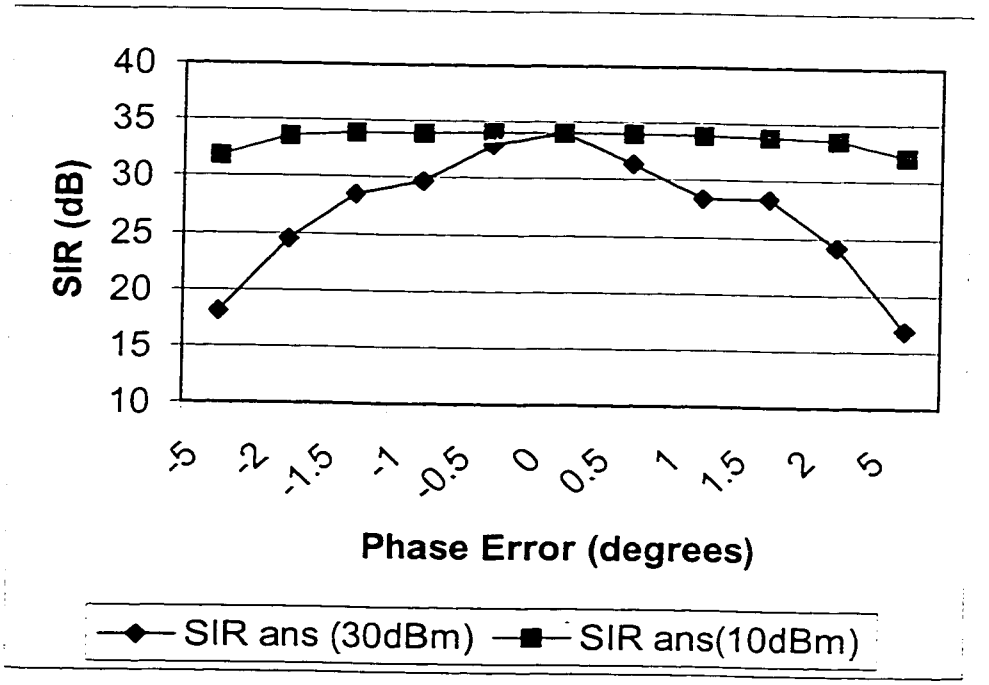

Figure 4.15: Effect of Phase error on RFI suppression.

Table 8: Impact of ANS Filter Phase Error on SIR levels.

ANS Gain Error	$SIR_{(30dBm\ RFI)}$	$SIR_{(10\ dBm\ RFI)}$
-2°	24.5236 dB	33.5769 dB
-1.5°	28.4885 dB	33.867 dB
-1°	29.6859 dB	33.9528 dB
-0.5°	32.862 dB	34.0158 dB
0°	34.0203 dB	34.0466 dB
0.5°	31.3468 dB	34.0079 dB
1°	28.3911 dB	33.9471 dB
1.5°	28.3273 dB	33.8265 dB
2°	24.2043 dB	33.551 dB

Bandpass filter 1 was used in all simulation cases presented in Table 8.

Phase error is difficult to control compared with gain error. As with gain error, phase error exhibits the same properties with respect to RFI levels. That is, for low levels of RFI noise, phase error has minimal impact on SIR gain provided by the ANS system. At high RFI injection levels, phase error dominates the SIR performance of the system. From the presented data, a phase error of ± 1% is acceptable if a loss of 6 dB in SIR performance can be tolerated.

4.2.4 Effect of Bandpass Filter Parameters on System Performance

The last test case group verifies the impact of non-ideal bandpass filtering of the CM signal. The effect on SIR is measured with respect to variations in bandpass filter bandwidth and filter roll-off rate. See Table 2, for filter parameters. Results of SIR performance vs. different RFI injection levels are presented in Table 9 and graphed in Figure 4.16. As well, results for SIR performance vs. loop balance are presented in Table 10 and graphed in Figure 4.17.

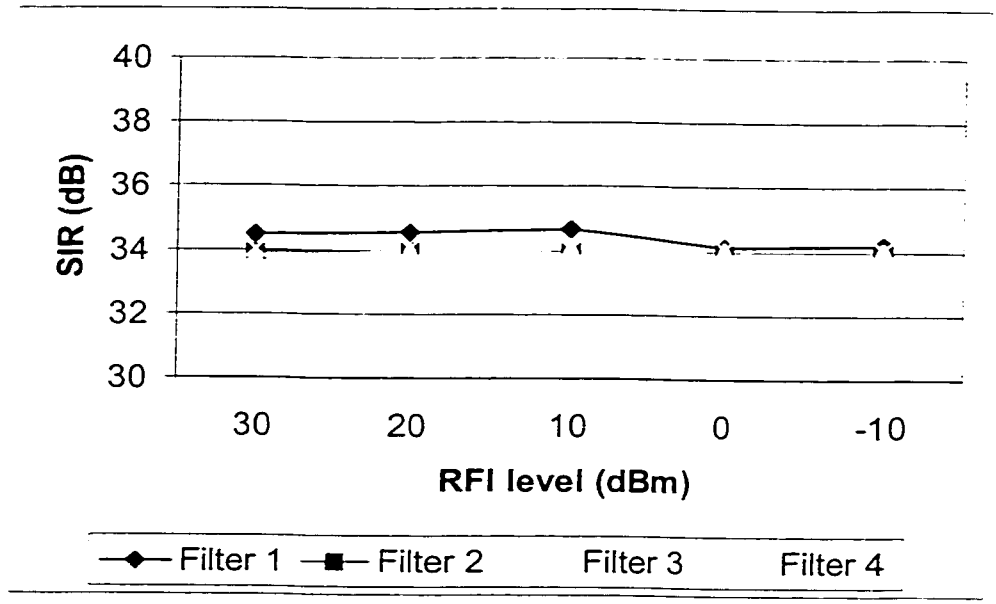

Figure 4.16: Performance of Bandpass filters w.r.t. RFI levels.

Table 9: Performance of Bandpass Filters on SIR vs. RFI levels.

RFI Level	Filter 1	Filter 2	Filter 3	Filter 4
30 dBm	34.4944 dB	33.905 dB	33.7563 dB	34.0158 dB
20 dBm	34.5696 dB	33.9864 dB	33.9925 dB	34.0573 dB
10 dBm	34.6465 dB	33.9956 dB	34.01 dB	34.0595 dB
0 dBm	34.139 dB	34.01 dB	34.0067 dB	34.0595 dB
-10 dBm	34.2054 dB	34.0086 dB	34.0075 dB	34.061 dB

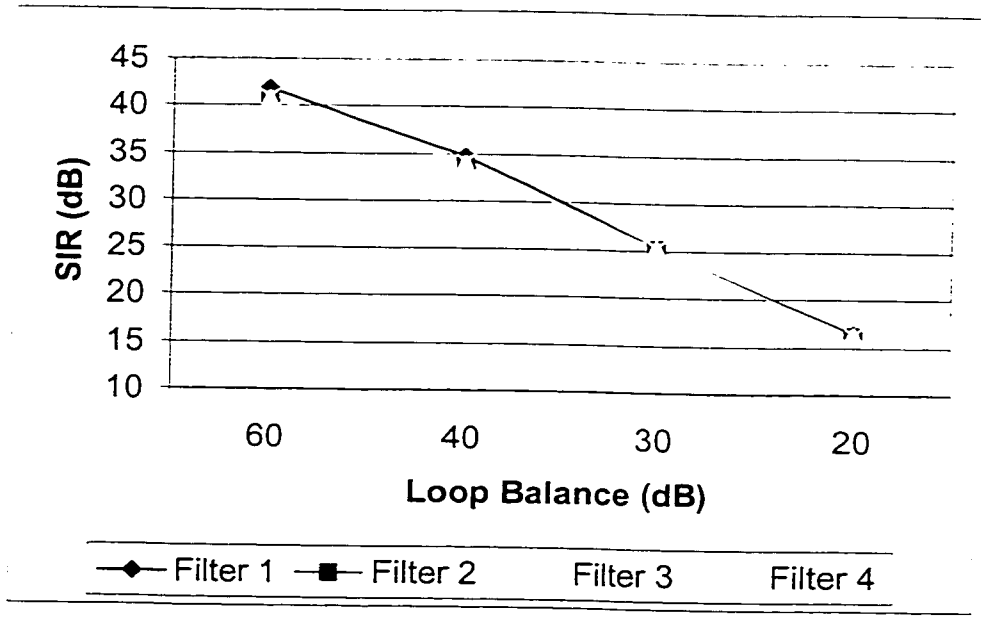

Figure 4.17: Performance of Bandpass filters w.r.t. Loop Balance.

Table 10: Performance of Bandpass Filters on SIR vs. Loop Balance.

Loop Balance	Filter 1	Filter 2	Filter 3	Filter 4
60 dB	41.8032 dB	40.8118 dB	40.7882 dB	40.8777 dB
40 dB	34.6465 dB	33.9956 dB	34.01 dB	34.0595 dB
30 dB	25.2787 dB	25.2307 dB	25.2301 dB	25.2416 dB
20 dB	16.4135 dB	16.3213 dB	16.3189 dB	16.2956 dB

Finally, this last experiment quantifies the effects of different filter bandwidth and roll-off rates on ANS system performance. Filters used in this simulation range from 185 kHz to 571 kHz in bandwidth and 400 dB/decade to 724 dB/decade in roll-off rate (see Table 2 for details). As shown in results of section 4.2.4, filter bandwidth and roll-off rate have very little effect on SIR. Therefore, an efficient (low order) filter can be used for bandpass filtering of the CM signal without severely impacting system performance.

4.3 Conclusion

Results from section 4.2.1 show that the RFI suppression performance of the ANS system is such that the SIR at the receiver increases to between 34 and 35 dB with ANS active irrespective of the initial SIR of the channel. (Assuming a loop balance of 40dB.)

Gain error has little effect on SIR for low RFI injection levels. Conversely for high RFI levels, the SIR figure is influenced by gain error such that signal level matching of the canceling and DM signals become critical. From the presented data, a gain error of ± 2% is tolerable for an impact of 4 to 5 dB on the SIR performance at 30 dBm RFI power levels.

As with gain error, phase error exhibits the same properties with respect to RFI levels. At high RFI injection levels, phase error dominates the SIR performance of the system. A phase error of ± 1% is acceptable if a loss of 6 dB in SIR performance can be tolerated at high RFI levels.

Filters used in this simulation range from 185 kHz to 571 kHz in bandwidth and 400 dB/decade to 724 dB/decade in roll-off rate (see Table 2 for details). As shown in results of section 4.2.4, filter bandwidth and roll-off rate have very little effect on SIR.

5 Summary and Future Work

Dominant common mode noise such as RFI ingress and Impulse noise will be reduced significantly. The noise reduction in a twisted-pair cable will increase the reach of digital subscriber loop modems and improve SNR, which allows higher signaling rate in the corresponding cable.

5.1 Applications

Although ANS is complementary to QAM, its use is not limited to this modulation technology. In fact ANS was designed with the intent to be modulation independent and transparent to the host technology. Therefore ANS could be applied to any modulation technique including DMT without requiring any modification to the modulation method or protocol. As a consequence, the implementation of ANS into DSL would not require deviating from established standards.

As well, ANS is not limited to ADSL or VDSL digital subscriber loop standards; this technique is capable of suppressing RFI for any other transmission technology that utilizes twisted pair cable as its transmission media. Therefore, this technique has potential application where twisted pair cable is subjected to high RFI environments.

5.2 *Limitations and Future Research*

ANS does not deal with impulse noise transients or cross-talk noise impairments as it is a narrow band filtering technique. Other signal conditioning techniques should be applied to deal with such impairments. Although limited to RFI, ANS successfully fulfills its intended application, the suppression of RFI noise to increase SIR (or SNR) for DM transmission on twisted pair loops. One area of research not investigated by the author is the application of multi-band ANS as a possible method of suppressing impulse noise.

Theoretically multi-band ANS could be composed of thousands of filter channels, but a practical implementation of an ANS system is constrained by technological limitation such as circuit complexity, size and inherent cost. As well special care must be taken in the selection of the target technology for the system, be it analog, digital or mixed signal. Each target technology provides advantages and pitfalls that must be considered for each specific implementation of ANS.

Additional research should be performed to evaluate other filter types, besides Butterworth filters, as candidates for the ANS filter channel bandpass filter. As well a fair amount of work is still required to define the control system for a realizable multi-channel ANS system and evaluate its performance when subjected to multiple RFI interferes. The RFI model developed in the VDSL standard [16] would be a good starting point to evaluate such a system.

1 Warner Jean-Jacques, Ahamed V. Syed, Gruber L. Patricia, "Digital Subscriber Line (HDSL and ADSL) Capacity of the Outside Loop Plant", IEEE Journal on Selected Areas in Communication, Vol. 13, No. 9, December 1995.

2 Cheng, David K., "Field and Wave Electromagnetics", Addison-Wesley, 1989, ISBN 0-201-12819-5.

3 Lee, K.F., "Principles of Antenna Theory", Wiley, New York, 1984.

4 This Model was developed at Nortel Networks with the participation of the Author and has subsequently been submitted to ANSI T1E1.4 (1996).

5 Miller G, "The Effect of Longitudinal Imbalance on Crosstalk", The Bell Systems Technical Journal, Vol. 54, No.7, September 1975.

6 Cook, John, "Parametric Modeling of Twisted Pair Cables for VDSL", T1E1.4/96-15, BT Laboratories, January 1996.

7 Whitham D. Reeve, "Subscriber Loop Signaling and Transmission Handbook Digital", IEEE Telecommunications Handbook Series, IEEE press, New York, 1995, ISBN 0-7803-0440-3.

8 Telecommunications Policy Branch, "Canadian Table of Frequency Allocations 9 kHz to 275 GHz", Industry Canada, 1998, Ottawa, ISBN 0-662-267753-3.

9 Whitham D. Reeve, "Subscriber Loop Signaling and Transmission Handbook *analog*", IEEE Telecommunications Handbook Series, IEEE press, New York, 1992, ISBN 0-87942-274-2.

10 Bellcore, "Carrier Service Area standard Test Loops", Bellcore standard TA-NWT-001210, Issue 1, October 1991.

11 Dominique St-Martin, Pierre Lefebvre, "RFI Drop Wire Characterization Ottawa – Repentigny", Nortel (Northern Telecom), 1996.

12 Humphrey, L.D., "RFI Related Requirements for VDSL", *Source*: Nortel, *Distribution*: ANSI T1E1.4 Technical Subcommittee Working Group, 1996, T1E1.4/96-031.

13 Richard A. Combellack, "Improving Range and Bandwidth of Telco Loop Plant", Proceedings of the 47th International Wire and Cable Symposium, Philadelphia, Pennsylvania, 16 – 19 November 1998.

14 Inkyu Lee, Jacky S. Chow, John M. Cioffi, "Performance Evaluation of Fast Computation Algorithm for the DMT in High-speed Subscriber Loop", IEEE Journal on Selected Areas in Communications, Vol. 13, No.9 December 1995.

15 John W. Cook, "Wideband Impulsive Noise Survey of the Access Network", BT Technology Journal, Vol. 11, no.3, July 1993, pp. 155-162.

16 T1E1.4 VDSL Editor, "Very-high-speed Digital Subscriber Lines – System Requirements", T1E1 committee group T1E1.4/98-043R8, Nov. 30 1998.

17 Thomas Starr, John Cioffi and Peter Silverman, "Understanding Digital Subscriber Line Technology, Prentice-Hall, 1999.

18 Jean-Jacques Werner, "The HDSL Environment", *IEEE Journal on Selected Areas in Communication*, vol. 9, no. 6, August 1991, pp. 785-800.

19 John Cioffi, ed. "Very-high-speed Digital Subscriber Lines - System Requirements", *ANSI Contribution T1E1.4/98-043R8*, Plano, Texas, 30 November 1998.

20 Jeffrey Rakos and Mahbub Hoque, "Ingress and Egress Model Analyses for Broadband Deployment", *ANSI Contribution T1E1.4/97-279 (Bellcore)*, 22 September 1997.

21 British Telecom presentation at "Very-high-speed Digital Subscriber Lines (VDSL) Workshop" (leader: John Cioffi), IEEE Global Communications Conference, Nov. 18 1996.

22 Whitham Reeve, *Subscriber Loop Signalling and Transmission Handbook - Digital*, IEEE Press, 1995.

23 John Cioffi, Mark Mallory, and John Bingham, "Analog RF Cancellation with SDMT", ANSI Contribution T1E1.4/96-084, 22 Apr. 1996.

24 Humphrey L. D., "Balance Measuremnts on BT Drop Wire 10", ANSI Contribution T1E1.4/95-144, Orlando, Florida, 13 Nov. 1995.

25 Richard Dorf, editor-in-chief, *The Electrical Engineering Handbook*, CRC Press, 1993.